Electronic Supplementary Material (ESI) for Dalton Transactions.

Zinc thiotropolone combinations as inhibitors of the SARS-CoV-2 main protease

Christopher R. DeLaney[a†], Yan Sheng[b†], D. Chase Pectol[a], Erol C. Vantansever[c], Hanyuan Zhang[b], Nattamai Bhuvanesh[a] , Isaiah Salas[a], Wenshe R. Liu*[c], Carol A. Fierke*[b] and Marcetta Y. Darensbourg*[a]

Abstract: Numerous organic molecules are known to inhibit the main protease of SARS-CoV-2, ($SC2M^{pro}$), a key component in viral replication of the 2019 novel coronavirus. We explore the hypothesis that zinc ions, *long used as a medicinal supplement and known to support immune function*, bind to the $SC2M^{pro}$ enzyme in combination with lipophilic tropolone and thiotropolone ligands, **L**, block substrate docking, and inhibit function. This study combines synthetic inorganic chemistry, *in vitro* protease activity assays, and computational modelling. While the ligands themselves have half maximal inhibition concentrations, IC_{50} values, for $SC2M^{pro}$ in the 8-34 μM range, the IC_{50} values are ca. 100 nM for $Zn(NO_3)_2$ which are further enhanced in Zn/**L** combinations (59-97 nM). Isolation of the $Zn(\mathbf{L})_2$ binary complexes and characterization of their ability to dissociate into $Zn(\mathbf{L})^+$ in the presence of suitable acceptors is the basis for computational modeling of the chemical features of the enzyme inhibition. Docking onto the $SC2M^{pro}$ enzyme surface using a modified Autodock4 protocol found preferential binding into the active site pocket. Such Zn-**L** combinations orient so as to permit dative bonding of $Zn(\mathbf{L})^+$ to basic active site residues.

DOI:

Table of Contents

I. Experimental Procedures

General materials and techniques

All air sensitive reactions were carried on a double manifold Schlenk vacuum line under N_2 with the resulting compounds stored under N_2 or Ar in a glovebox. Chloroform, Dichloromethane, diethylether, hexanes, pentane, and methanol were freshly purified by an MBraun Manual solvent purification system packed with Alcoa F200 activated alumina desiccant. Reagents were purchased from commercial sources and used as received. Syntheses for 7-Oxocyclohepta-1,3,5-trien-1-yl 4-methylbenzenesulfonate (Tosyl-**L1**),[3] 6-(1-Methylethyl)-2-[[(4-methylphenyl)sulfonyl]oxy]-2,4,6-cycloheptatrien-1-one (Tosyl-**L3**),[4] 4-(1-Methylethyl)-2-[[(4-methylphenyl)sulfonyl]oxy]-2,4,6-cycloheptatrien-1-one (Tosyl-**L2**),[4] 2-Mercaptotropone (**L1**),[5] 2-Hydroxy-4-isopropylcyclohepta-2,4,6-triene-1-thione (**L3**), 7-Hydroxy-3-isopropylcyclohepta-2,4,5-triene-1-thione (**L2**),[4] Zn(Tropolone)$_2$,[6] Zn(Hinokitiol)$_2$,[6] 4(5)-(2-haloethyl)imidazole hydrochloride,[7] and 4(5)-(2(-S-thiouronium)ethyl)imidazole hydrochloride (NS-mimic)[7] were carried out according to established procedures.

Physical Measurements

Nuclear Magnetic Resonance Spectroscopy was carried out using a 400MHz NMR spectrometer. Ultraviolet-visible spectroscopy was performed on a Shimadzu UV-2450 spectrophotometer. Mass Spectrometry (ESI-MS and ACPI-MS) were performed in the Laboratory for Biological Mass Spectrometry at Texas A&M University. Data collections for X-ray structure-determination were carried out BRUKER Quest X-ray (fixed-Chi geometry) diffractometer with a PHOTON II detector with X-ray radiation generated by a Mo-Iμs X-ray tube (K_α = 0.71073Å). Crystals were coated in paraffin oil and mounted on a nylon loop, and placed under streaming N_2 (110/150K). Integrated intensity information for each reflection was obtained by reduction of the data frames with the program APEX3.The structure was refined (weighted least squares refinement on F^2) to convergence. Mercury and OLEX were employed for the final data presentation and structure plots.

Lipophilicity determination for Zn complexes

Octanol-water partition coefficients were obtained as following established protocols.[8] For **L1**, a stock solution in 1-octanol (pre-equilibrated with Phosphate Buffered Saline pH = 7.4) was created and used to establish a standard curve. Partition experiments were conducted by shaking 5 mL the 1-octanol solutions of **L1** with an equal volume of PBS for 1 hour, followed by separation for an additional hour. The absorbance at 420 nm of the organic layer was measured as was that of the PBS layer. This was repeated with fresh solutions, with 0.5 eq of $Zn(OAc)_2$ dissolved in the PBS before partition. The ratio of the absorbance in the organic and aqueous layers was used to calculate the partition coefficients. For the intact complexes, a standard curve of known concentrations of each Zn-complex was established in PBS saturated 1-octanol. Next, 5 mL aliquots of the most concentrated Zn(**L**)$_2$ solutions were transferred to separatory funnels, at which point 45 mL of the pre-equilibrated PBS was added for a total volume of 50 mL. These flasks were shaken for 1 hour before being allowed to rest for an additional hour to ensure separation of the phases. A sample of the organic layer was taken for analysis via UV-Vis and the partition coefficient calculated as previously described. All trials were completed in triplicate.

Inhibition analysis

Recombinant SC2M^{pro} protein was expressed and purified according to literature protocol.[9] The protein was then changed into buffer A (20 mM HEPES, 10 mM NaCl, pH 7.8) using a spin desalting column (Zeba). The purified SC2M^{pro} was diluted to 10 μM in buffer A (as determined by a Pierce 660 nm assay) and stored at -80 °C. The inhibition assay was based on the established fluorescent peptide assay system[9]. The FRET-based tetradecapeptide substrate (DABCYL-Lys-Thr-Ser-Ala-Val-Leu-Gln-Ser-Gly-Phe-Arg-Lys-Met-Glu-EDANS) was purchased from Bachem and stored as a 1 mM solution in 100% DMSO. All inhibitors were stored as 10 mM in 100% DMSO solutions in -20 °C freezer. The final inhibition assay contained 50 nM M^{Pro}, 10 μM substrate, and varying concentrations of inhibitors. Enzyme and substrate stock solutions were diluted using buffer A. Inhibitors were diluted into varying concentrations maintaining 10% DMSO in buffer A. 40 μL of a 62.5 nM SC2M^{Pro} solution was added to each well in a 96-well plate, and 5 μL of inhibitor solution with varying concentrations was added. After a brief shaking, the plate was incubated at 37°C for 15 min. Then 5 μL of a 100 μM substrate solution was added to initiate the activity analysis. The EDANS fluorescence with excitation at 336 nm and emission at 490 nm from the cleaved substrate was detected. The slope from the time-dependence of the fluorescence increase was determined for 10 min. **Equation S1** was fit to the dependence of the initial rate on the inhibitor concentration to determine the value of the IC_{50} and n = Hill coefficient (cooperativity factor). GraphPad 8.0 was used to analyze the data and the standard error of the mean via ANOVA. The value of n varies from 0.6-3.7 for ligands (**L**) and varies from 1.4-2.0 for $Zn(NO_3)_2$ and Zn(**L**)$_2$ complexes**.**

Equation S1: % Activity = $100\%/(1+([I] / IC_{50})^n)$

Computational Methods

AutoDock4 was used for blind docking and for the generation of binding poses. The protein used in this study was the monomer of the COVID-19 main protease (PDB:6W63) with the inhibitor X77 and water removed. For each potential inhibitor, **L**, Zn(**L**)$^+$, and

$Zn(\mathbf{L})_2$, the genetic algorithm-based calculation was performed with 20 runs for the blind docking, and 100 runs for the active site docking with the output being in Lamarckian Genetic Algorithm form. The rest of the parameters are as follows: Population Size: 150, Max. number of evaluations: 2.5 million, Max. number of generations 27000, rate of crossover: 0.8. The **L** and $Zn(\mathbf{L})^+$ molecules used in these simulations were truncated forms of the $Zn(\mathbf{L})_2$ crystal structures for **L1** and **L2**. The charges on all potential inhibitors were generated using an AM1-BCC forcefield. For the coordinatively unsaturated Zn(**L**)+, the charge of the ligand was calculated, and then charge was assigned to the metal to align with the charge of the fragment (i.e., if the total charge of the **L** was -1, and the known charge of the metal-containing fragment was +1, then the charge assigned to the Zn would be +2). Since no crystal structures exist for the $Zn(\mathbf{L3})_2$ complex, the bis-ligated complex was generated using the Structure Editing tools in UCSF Chimera. This $Zn(\mathbf{L3})_2$ was then truncated in an analogous manner to generate **L3** and $Zn(\mathbf{L3})^+$.

II. Syntheses and Characterization

Syntheses

$Zn(2\text{-Mercaptotropone})_2$ [$Zn(\mathbf{L1})_2$]

This preparation was adapted from Murakami et al.[5] A methanolic solution containing 205 mg (0.94 mmol) of $Zn(OAc)_2 \cdot 2H_2O$ was added via cannula to a stirred methanolic solution of **L1** (288 mg, 2.07 mmol). The resulting solution was then heated to 60°C and stirred vigorously for 3h before being allowed to cool to 22°C with stirring overnight. Stirring ceased and the orange precipitate was allowed to settle. The supernatant was then decanted via and the solid washed 2 times with additional methanol. The remaining solid was taken to dryness under vacuum and the resulting yellow/orange solid suspended in minimal diethyl ether. Cold (-20°C) pentane was then added to precipitate a yellow solid. The supernatant was then removed via canula and the solid was then washed twice more with cold pentane to remove excess ligand followed by purging with N_2 before drying *in vacuo*. (yield: 256 mg (80.2%)) Crystals suitable for XRD were obtained by slow evaporation of a filtered DCM solution saturated with the compound. $^+$APCI-MS (*m/z*): 338.94. $[M+H]^+$ ^{1}H NMR (400MHz $CDCl_3$): *δ* 8.68(1H, m), 7.58(1H, d) 7.48(1H, m) 7.26(2H, m). Elemental Analysis: Calc'd for $C_{14}H_{10}S_2O_2Zn$: C, 49.50 H, 2.97 S, 18.87; Found: C, 48.72 H, 3.02 S, 18.33.

$Zn(7\text{-Hydroxy-3-isopropylcyclohepta-2,4,5-triene-1-thione})_2$ [$Zn(\mathbf{L2})_2$]

A methanolic solution containing 46 mg (0.2 mmol) of $Zn(OAc)_2 \cdot 2H_2O$ was added via cannula to a stirred methanolic solution of **L2** (75 mg, 0.4 mmol). The resulting solution was then heated to 60°C and stirred vigorously for 3h before being allowed to cool to 22°C with stirring overnight. Stirring ceased and the orange precipitate was allowed to settle. The supernatant was then decanted via cannula and the solid washed 2 times with additional methanol. The remaining solid was taken to dryness under vacuum and the resulting yellow/orange solid suspended in minimal diethyl ether. Cold (-20°C) pentane was then added to precipitate a yellow solid. The supernatant was then removed via canula and the solid was then washed twice more with cold pentane to remove excess ligand followed by purging with N_2 then drying *in vacuo* (yield: 46.5 mg (53%)). Crystals suitable for XRD were obtained by slow evaporation of a filtered $CDCl_3$ solution of the compound. $^+$APCI-MS (*m/z*): 423.04. $[M+H]^+$ ^{1}H NMR (400MHz, $CDCl_3$) δ 8.72(1H, s), 7.39(2H, m), 7.10(1H, d), 2.87(1H, m), 1.24(6H, d). Elemental Analysis: Calc'd for $C_{20}H_{22}S_2O_2Zn$: C, 56.67 H, 5.23 S, 15.13; Found: C, 56.50 H, 5.16 S, 14.96.

$Zn(2\text{-Hydroxy-4-isopropylcyclohepta-2,4,6-triene-1-thione})_2$ [$Zn(\mathbf{L3})_2$]

A methanolic solution containing 140 mg (0.64 mmol) of $Zn(OAc)_2 \cdot 2H_2O$ was added via cannula to a stirred methanolic solution of **L3** (234 mg, 1.3 mmol). The resulting solution was then heated to 60°C and stirred vigorously for 3h before being allowed to cool to 22°C with stirring overnight. Stirring ceased and the orange precipitate was allowed to settle. The supernatant was then decanted via cannula and the solid washed 2 times with additional methanol. The remaining solid was taken to dryness under vacuum and the resulting yellow/orange solid suspended in minimal diethyl ether. Cold (-20°C) pentane was then added to precipitate a yellow solid. The supernatant was then removed via canula and the solid was then washed twice more with cold pentane to remove excess ligand followed by purging with N_2 then drying *in vacuo* (yield: 137.5 mg (51%)). $^+$APCI-MS (*m/z*): 423.04. $[M+H]^+$ ^{1}H NMR (400MHz, $CDCl_3$) δ 8.53(1H, s), 7.57(1H, s) 7.17(2H, s), 2.88(1H, m), 1.24(6H, d).

[Zn(**L1**)(Histidine)]

This reaction is representative of all the ligand displacement reactions involving $Zn(\mathbf{L1})_2$. A methanolic solution containing 60 mg (0.4 mmol) of L-Histidine was added via cannula to a stirred methanolic suspension of $Zn(\mathbf{L1})_2$ (34 mg 0.1 mmol). This suspension was allowed to stir overnight at 22°C resulting in an orange solution. This solution was taken to dryness *in vacuo* and the resulting orange solid washed with copious amounts of diethyl ether and then chloroform till washes were clear. Purging with N_2 followed by drying *in vacuo* resulted in a yellow powder (yield: 15 mg (42.1%)). $^+$ESI-MS (*m/z*): 356.00. $[M]^+$ ^{1}H NMR (400MHz, MeOH-d_4) δ 8.61(1H, s), 7.91(1H, s) 7.72(1H, s), 7.48(1H, m), 7.41(1H, d), 7.22(2H, m), 7.01(1H, s) 3.85(1H, m), 3.21(2H, m).

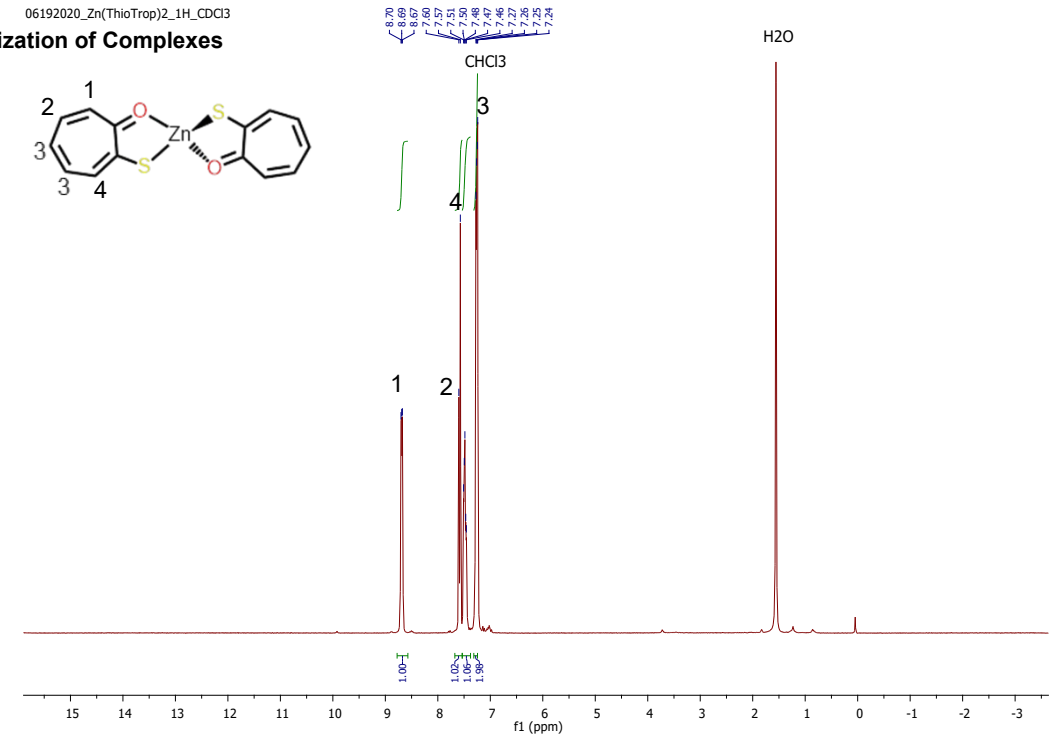

Figure S1. ^{1}H NMR spectrum of Zn(**L1**)$_2$ in $CDCl_3$ using a 400MHz NMR spectrometer referenced to TMS via residual $CHCl_3$.

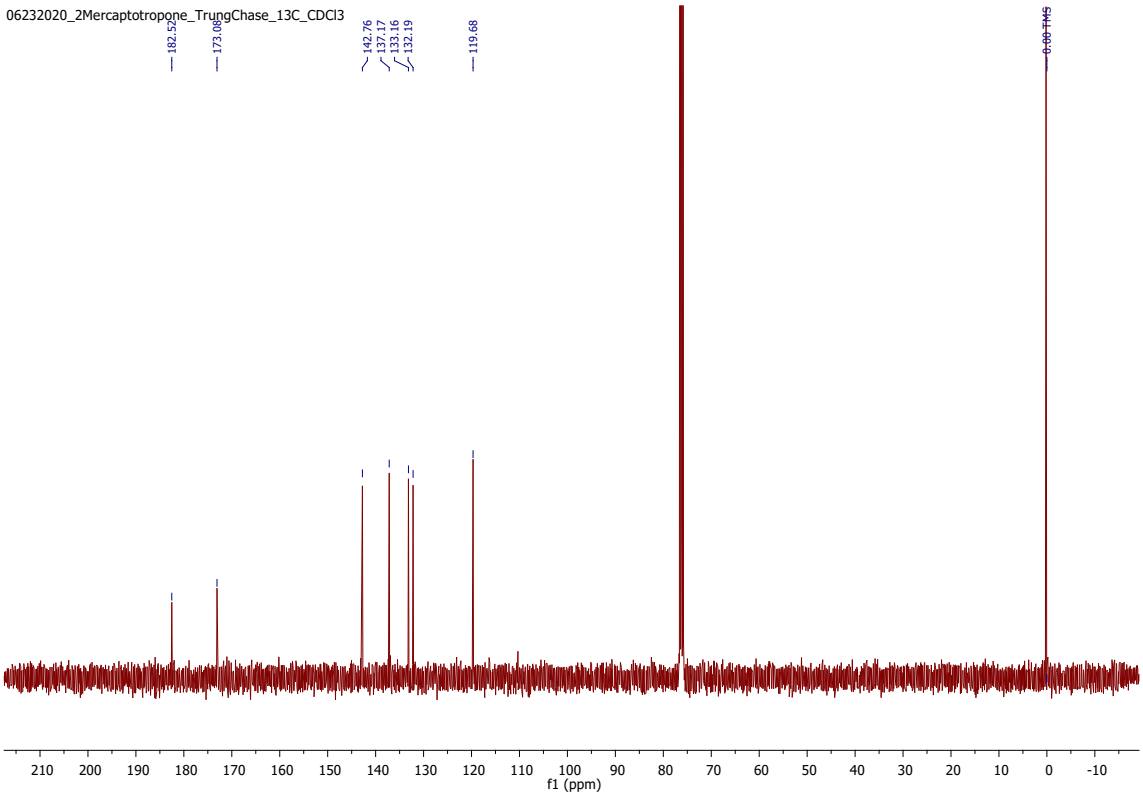

Figure S2. ^{13}C NMR spectrum of Zn(**L1**)$_2$ in $CDCl_3$ using a 100MHz NMR spectrometer referenced to TMS.

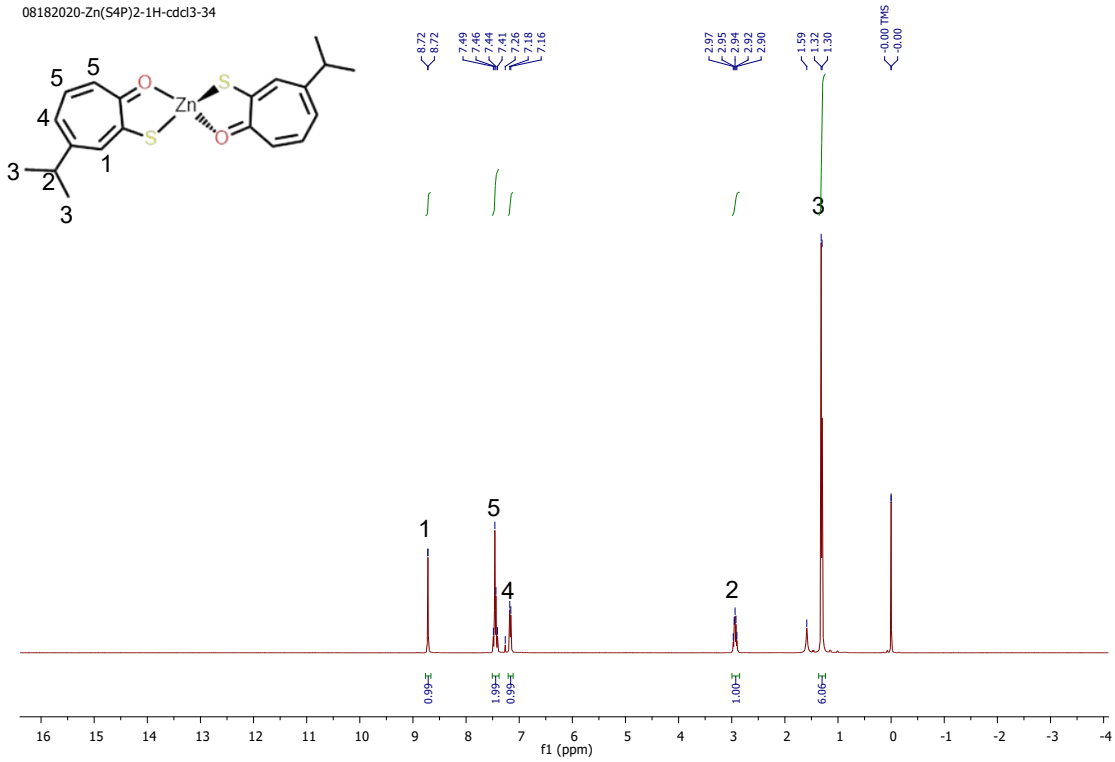

Figure S3. ^{1}H NMR spectrum of Zn(**L2**)$_2$ in $CDCl_3$ using a 400MHz NMR spectrometer referenced to TMS.

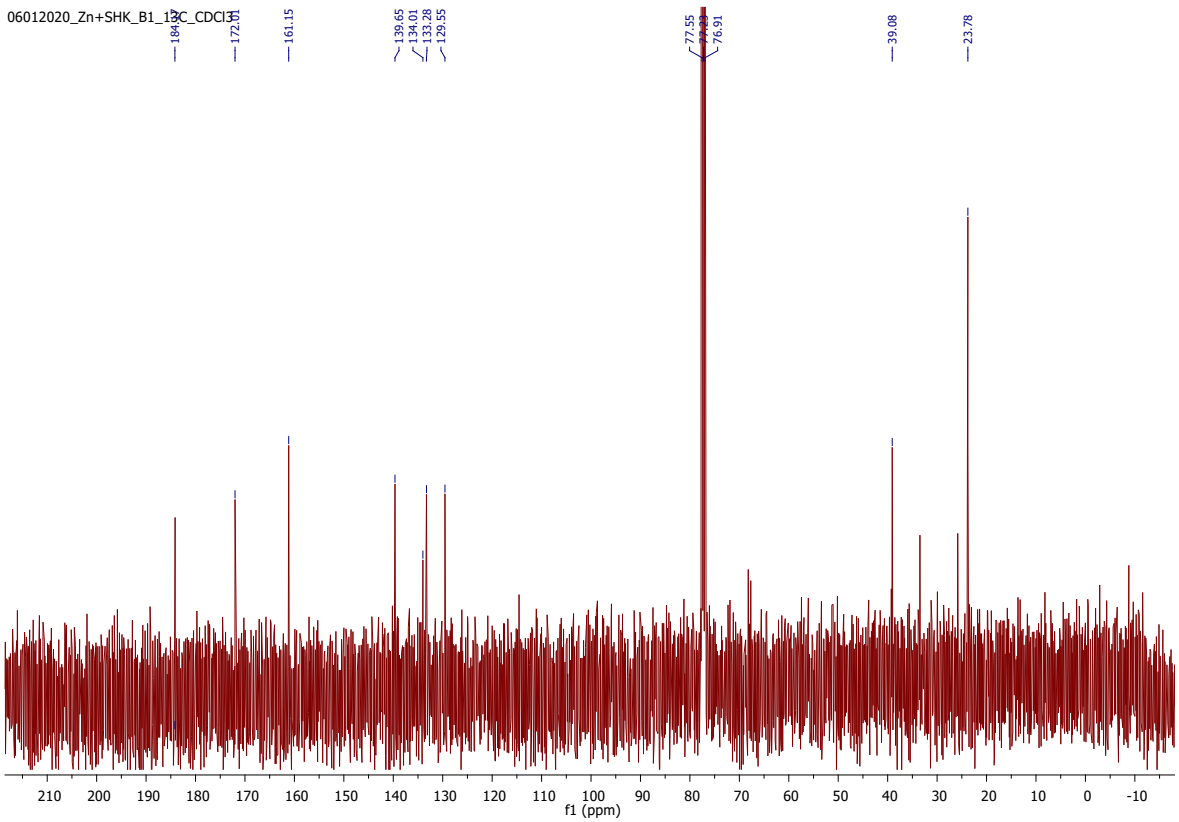

Figure S4. ^{13}C NMR spectrum Zn(**L3**)$_2$ in $CDCl_3$ using a 100MHz NMR spectrometer referenced to $CDCl_3$.

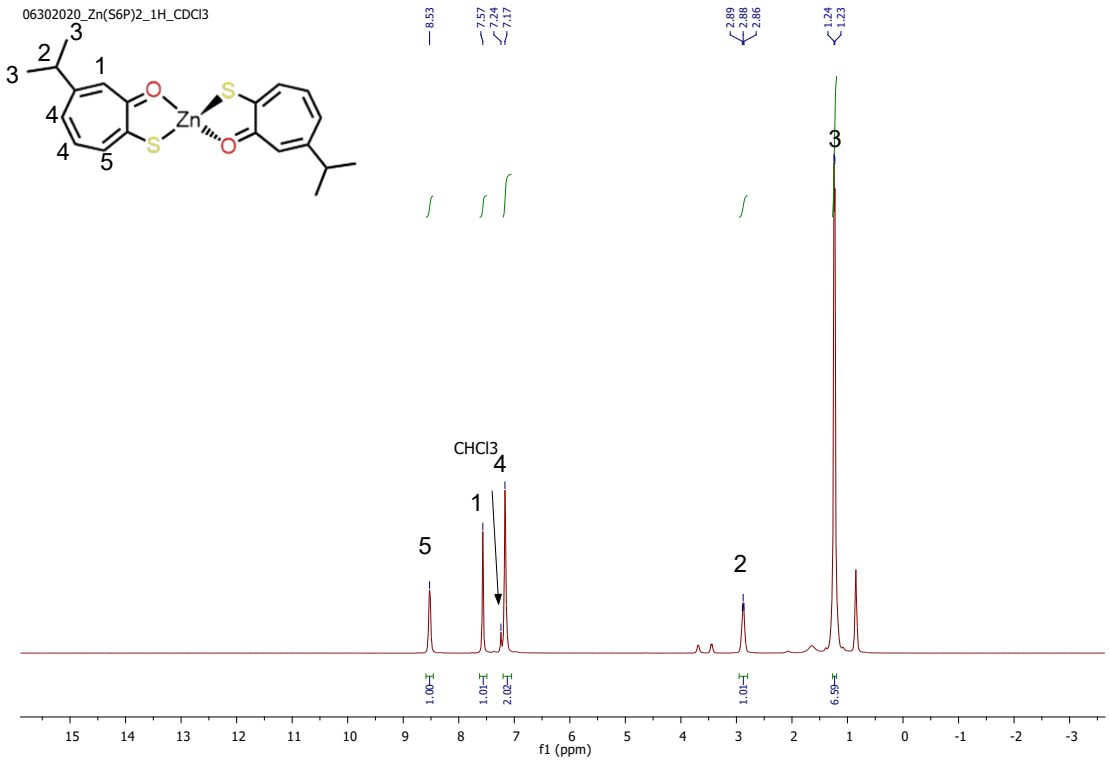

Figure S5. ^{1}H NMR spectrum Zn(**L3**)$_2$ in $CDCl_3$ using a 400MHz NMR spectrometer referenced to TMS via residual $CHCl_3$.

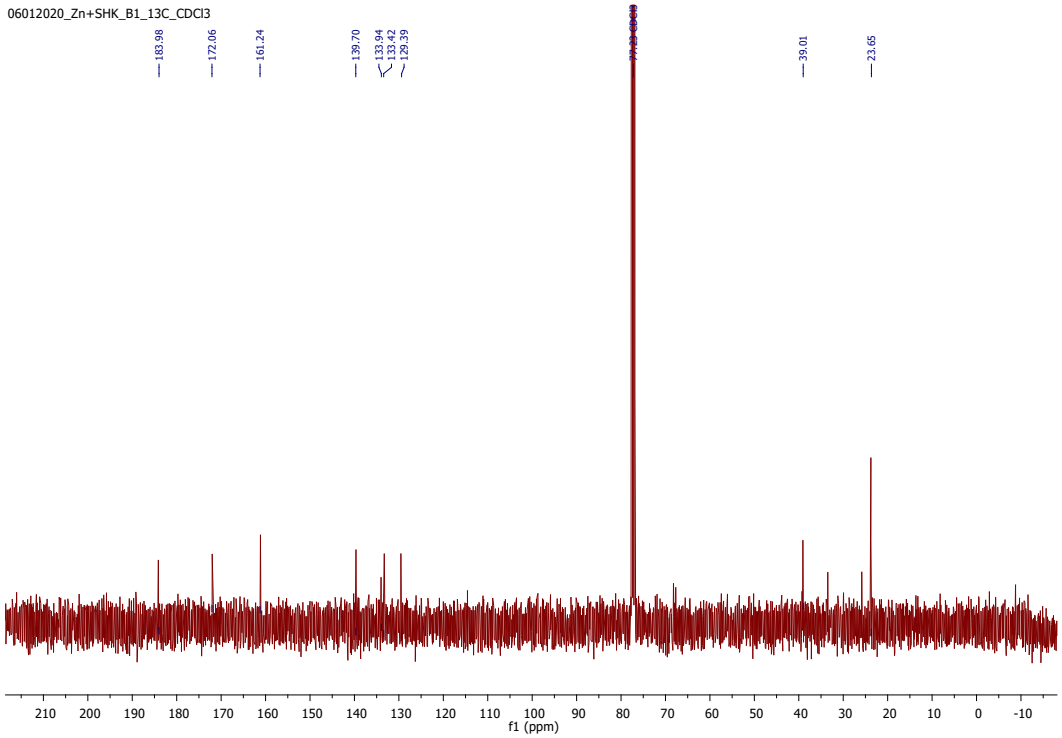

Figure S6. ^{13}C NMR spectrum Zn(**L3**)$_2$ in $CDCl_3$ using a 100MHz NMR spectrometer referenced to $CDCl_3$.

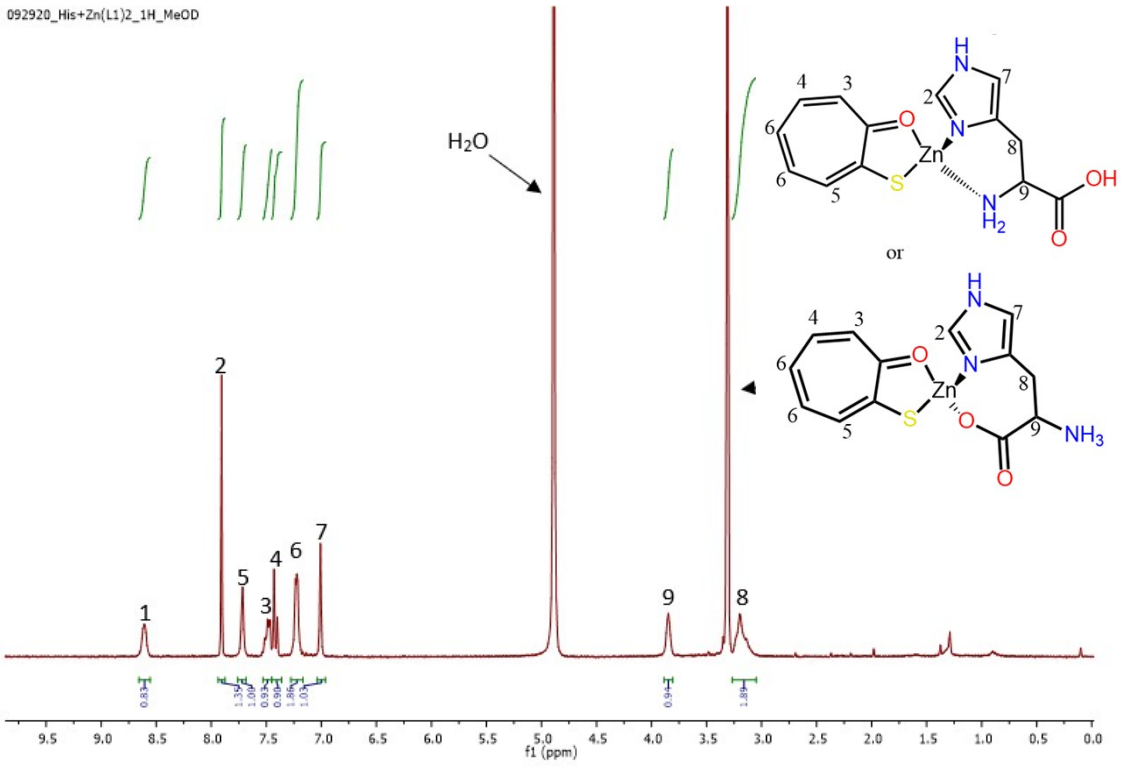

Figure S7. ^{1}H NMR of the reaction of Zn(**L1**)$_2$ with L-Histidine in MeOH-d$_4$ referenced to TMS via residual MeOH with a potential structure of the adduct given.

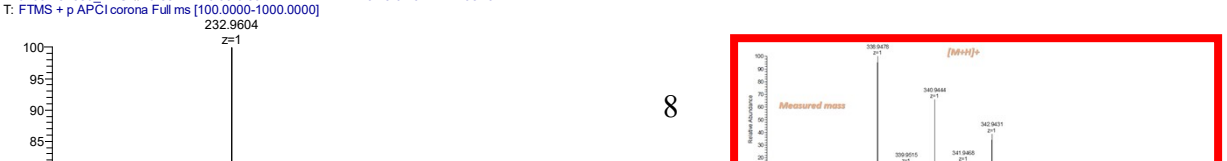

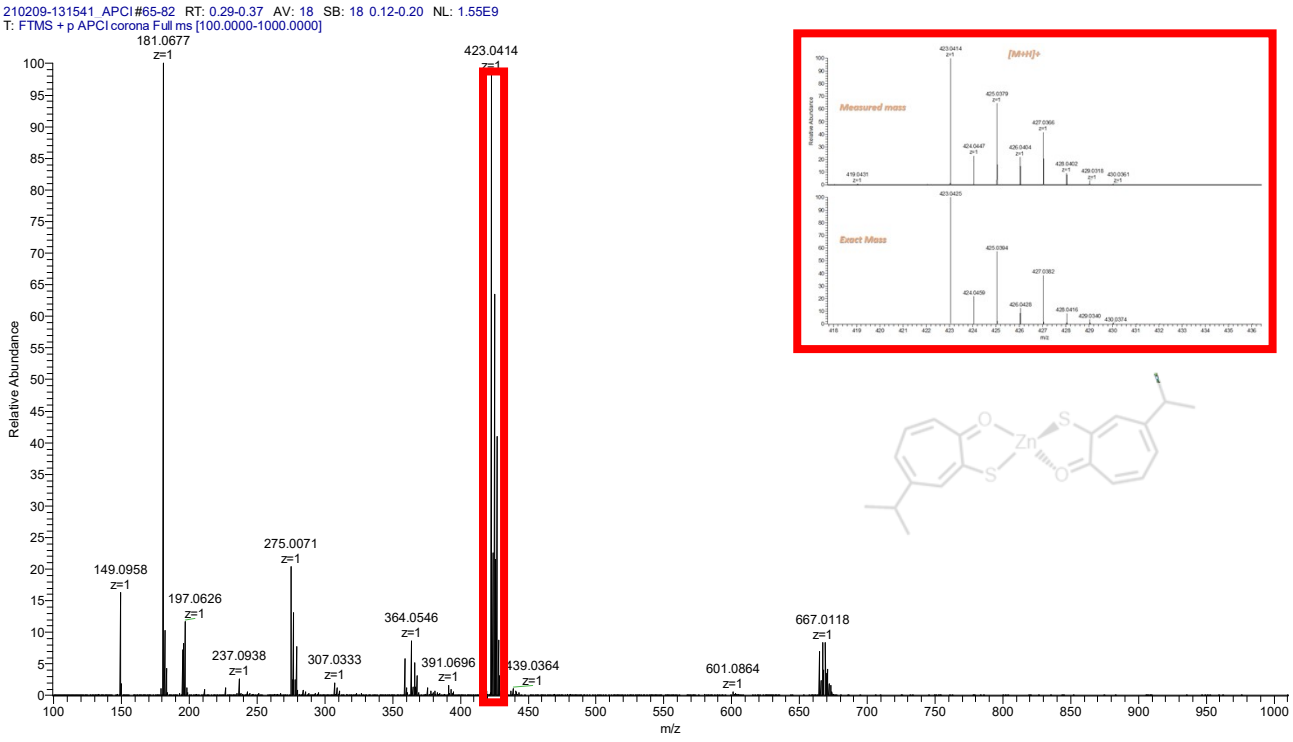

Figure S9. High resolution $^{+}$APCI-MS of Zn(**L2**)$_2$ in $CDCl_3$ with isotopic bundle for the parent ion. (Calc. for $[M+H]^+$ 423.04)

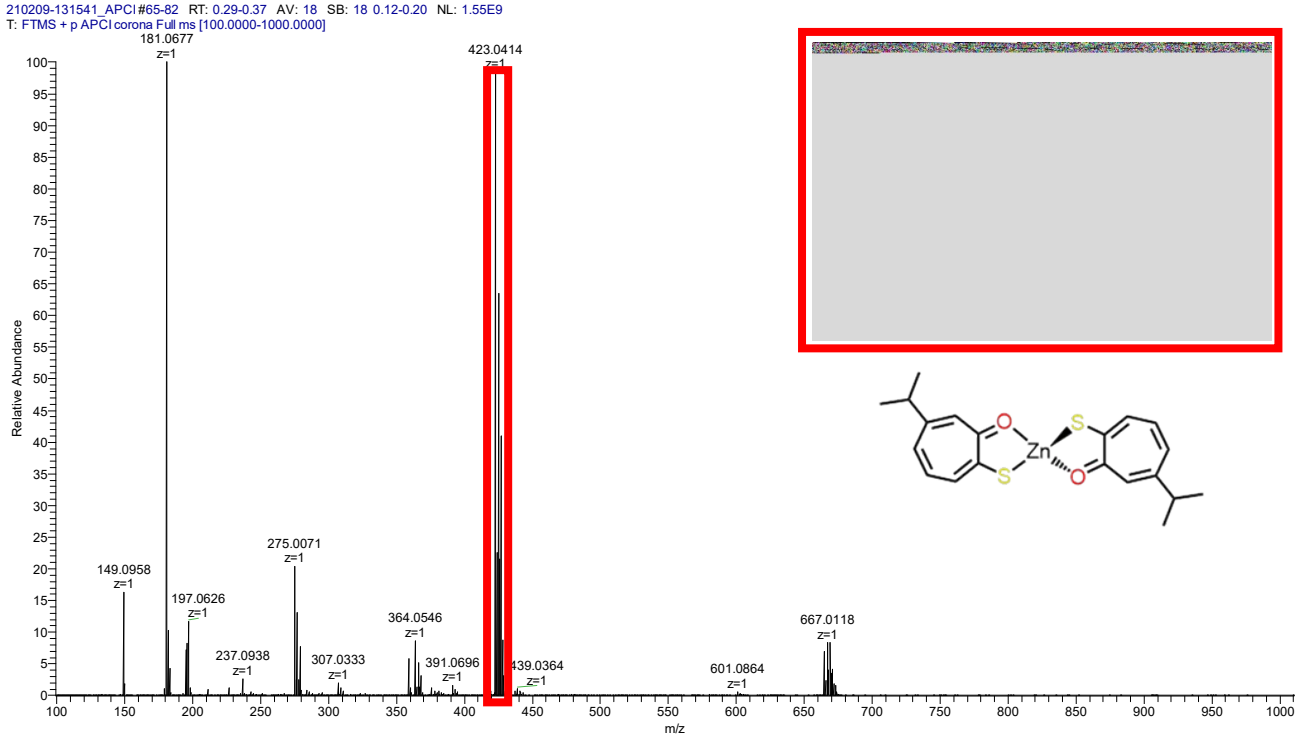

Figure S10. High resolution $^{+}$APCI-MS of Zn(**L3**)$_2$ in $CDCl_3$ with isotopic bundle for the parent ion. (Calc. for $[M+H]^+$ 423.04).

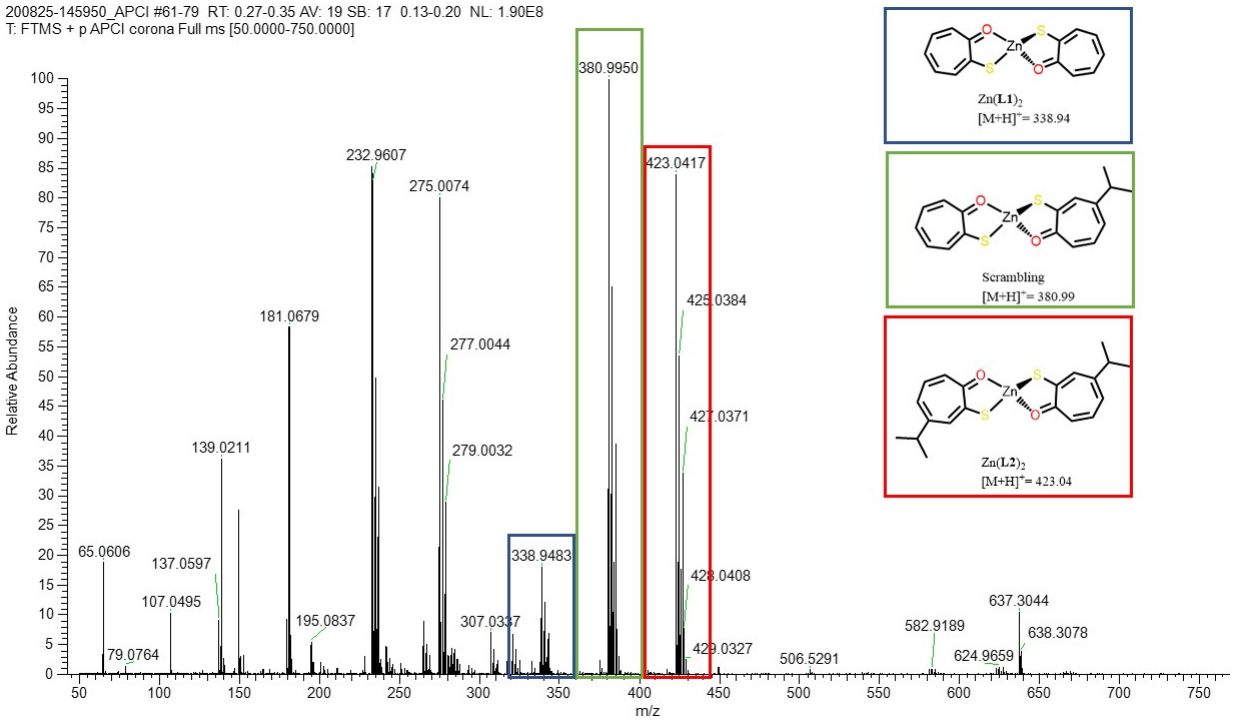

Figure S11. High resolution $^{+}$APCI-MS the reaction of Zn(**L1**)$_2$ with Zn(**L2**)$_2$ in DCM with isotopic bundles of interest highlighted Zn(**L1**)$_2$ in blue (Calc. for $[M+H]^+$ 338.94), Zn(**L1**)(**L2**) in green (Calc. for $[M+H]^+$ 380.99), and Zn(**L2**)$_2$ in red (Calc. for $[M+H]^+$ 423.04).

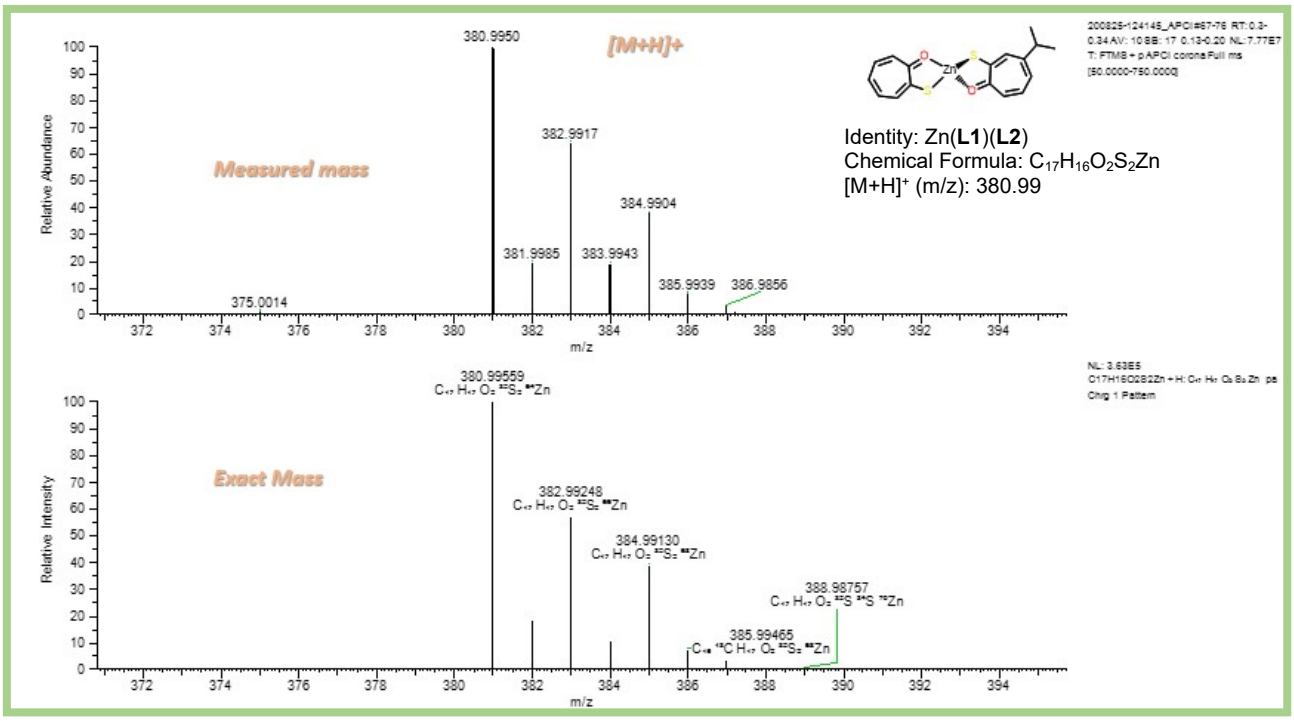

Figure S12. Isotopic bundle of scrambling product Zn(**L1**)(**L2**) (Calc. for $[M+H]^+$ 380.99) from **Figure S11** (green box) enlarged for clarity

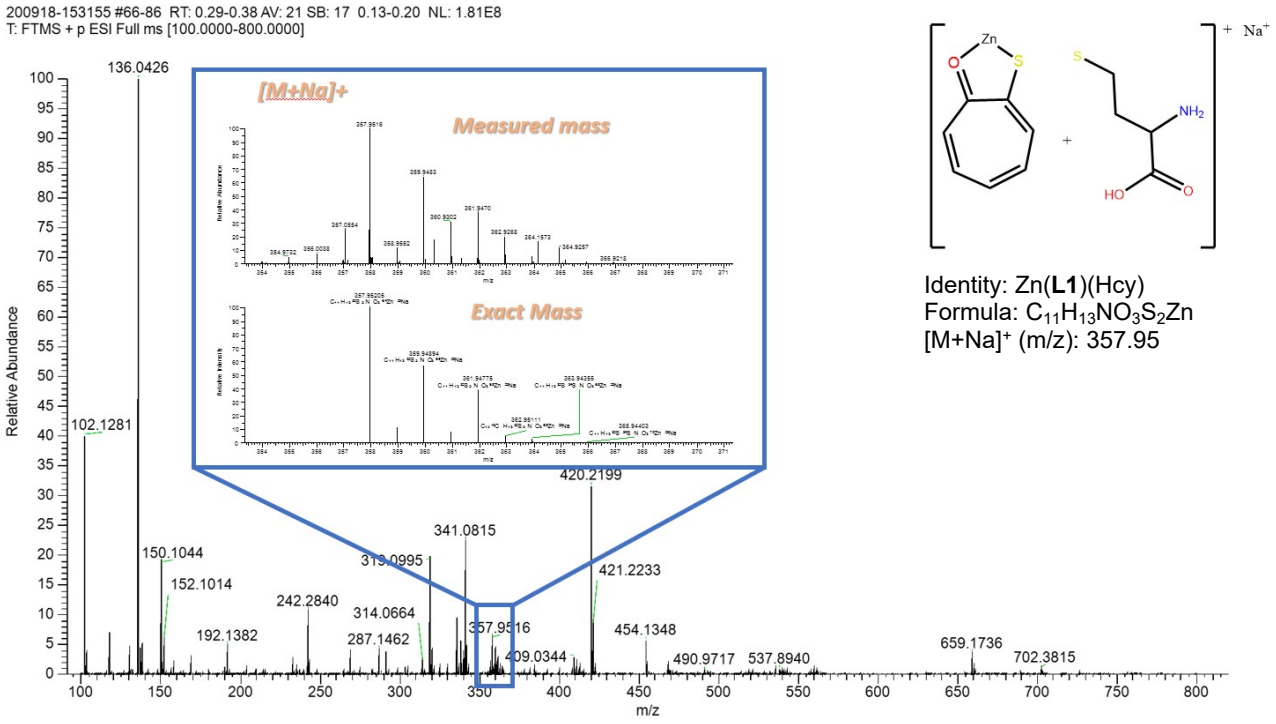

Figure S13. High resolution $^+$ESI-MS of reaction of Zn(**L1**)$_2$ with D,L-Homocysteine. Isotopic bundle ($[M+Na]^+$ 357.95) of interest highlighted in blue.

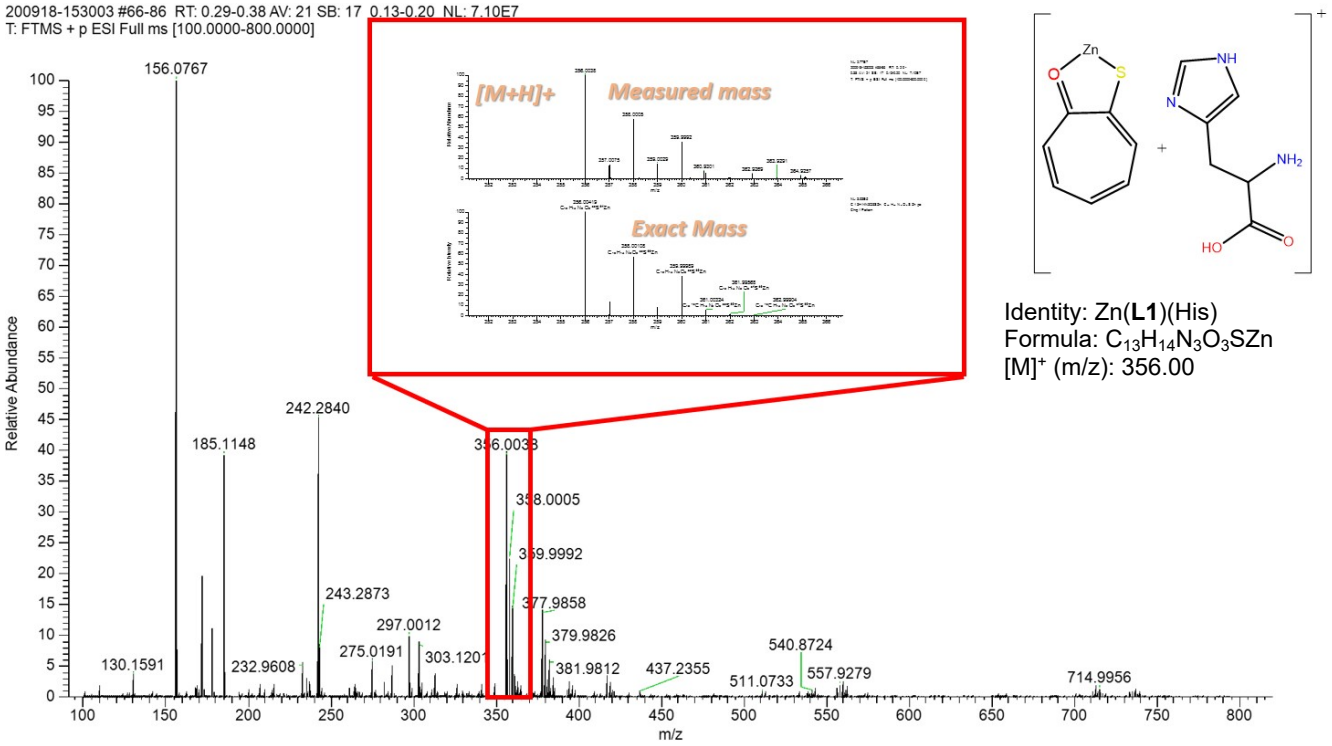

Figure S14. High resolution $^{+}$ESI-MS of reaction of Zn(**L1**)$_2$ with L-Histidine. Isotopic bundle ([M]$^{+}$ 356.00) of interest highlighted in red.

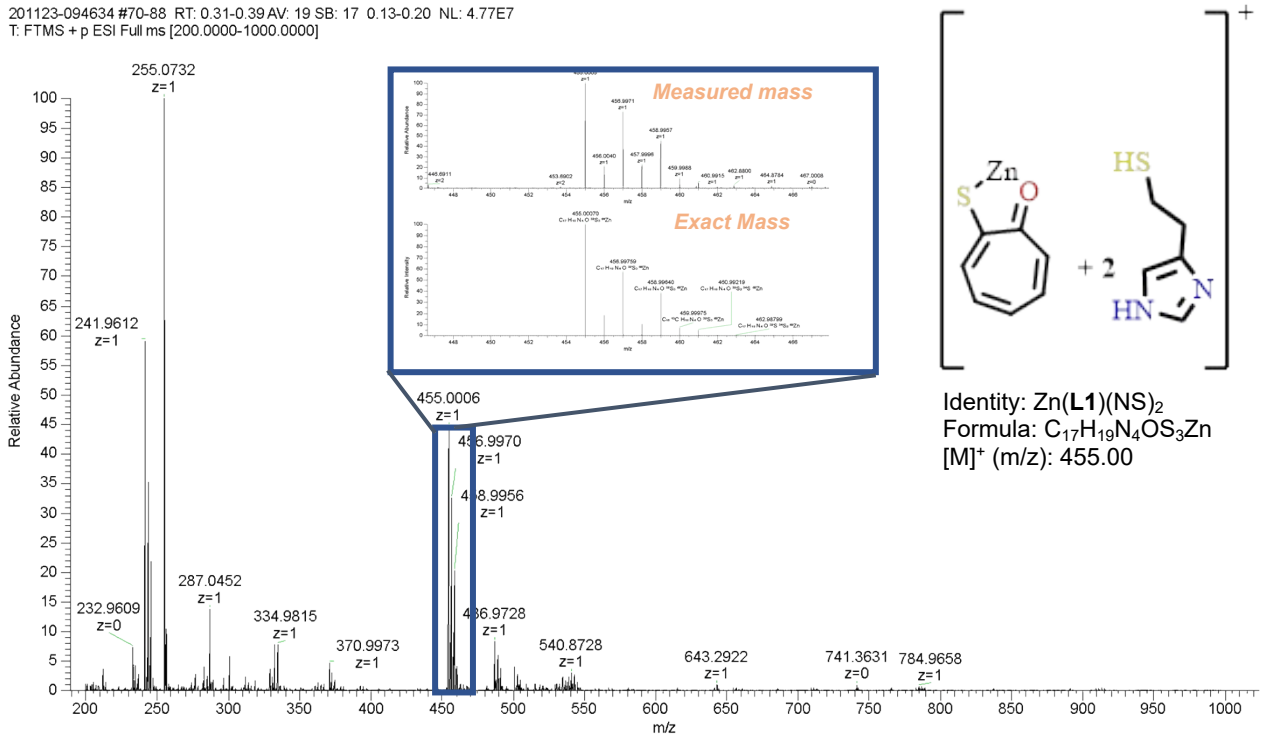

Figure S15. High resolution $^{+}$ESI-MS of reaction of Zn(**L1**)$_2$ with proposed NS-mimic. Isotopic bundle ([M]$^{+}$ 455.00) of interest highlighted in blue.

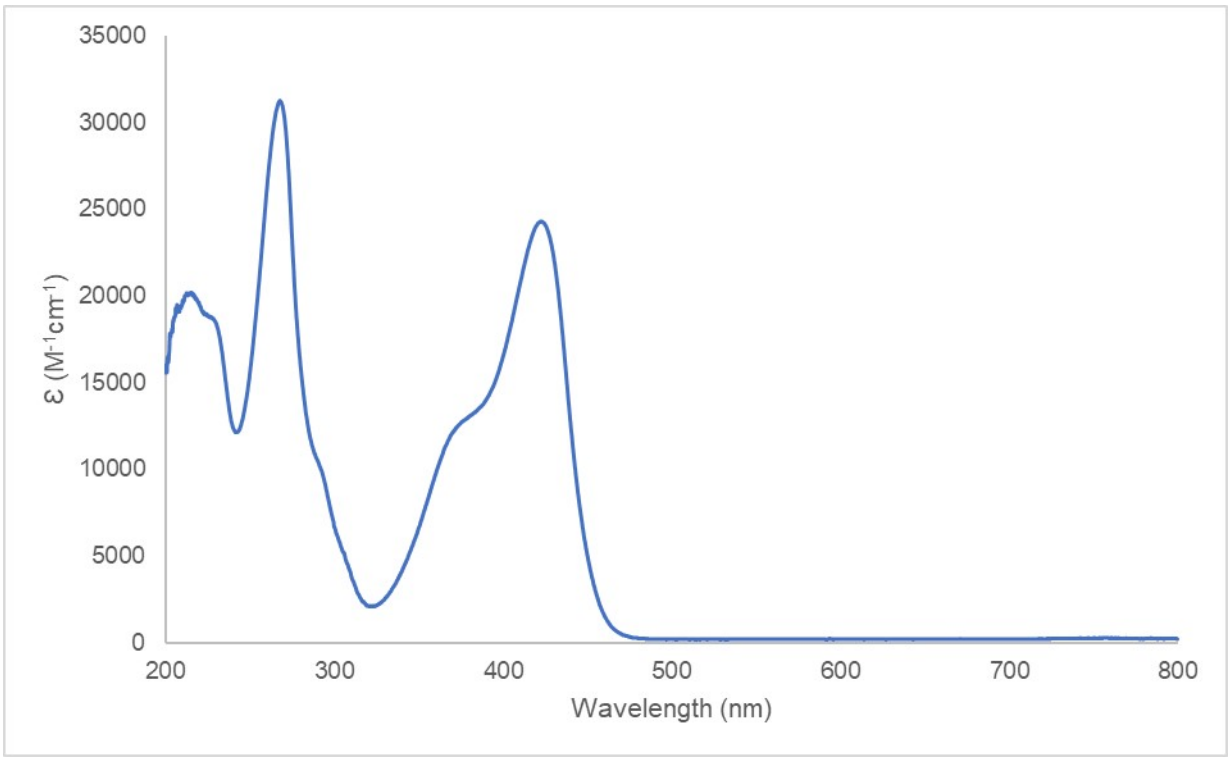

Figure S16. UV-Vis spectrum of Zn(**L1**)$_2$ in DCM.

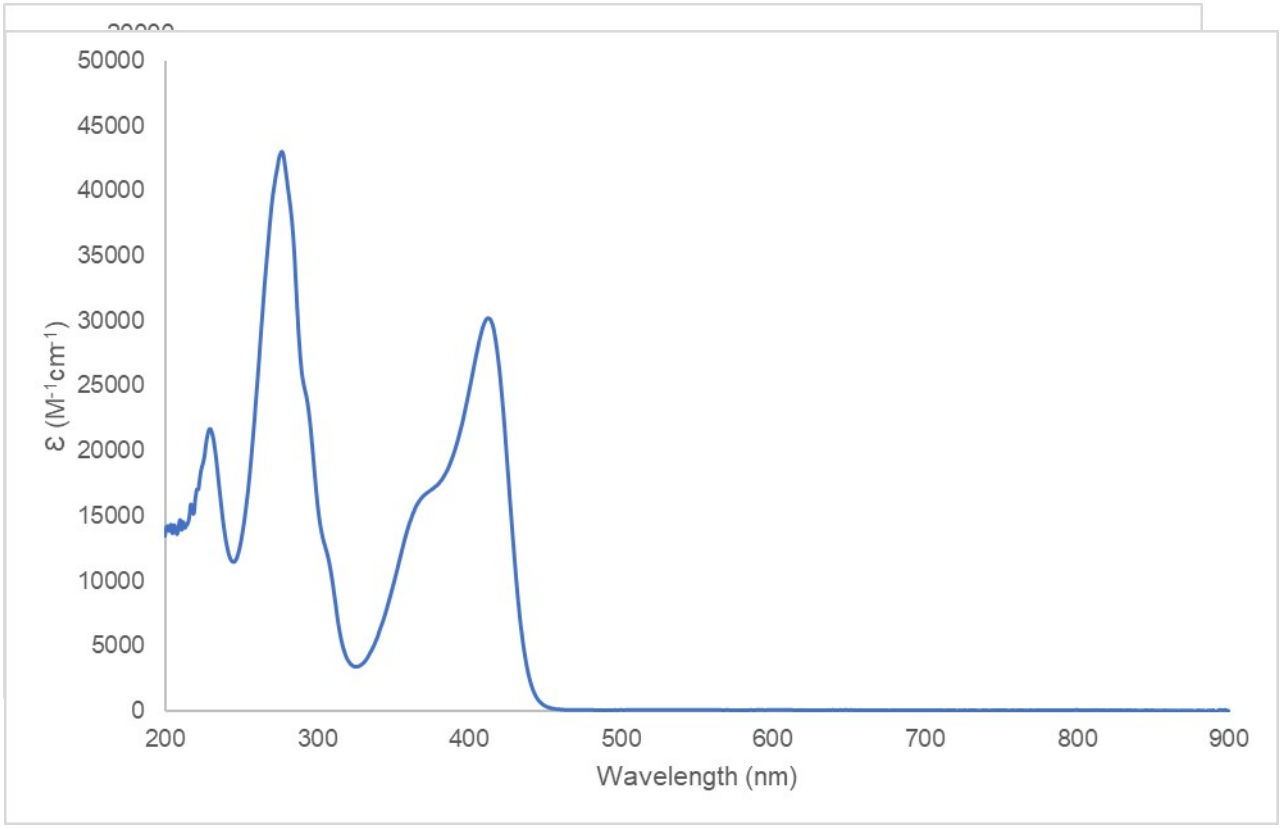

Figure S17. UV-Vis spectrum of Zn(**L2**)$_2$ in DCM.

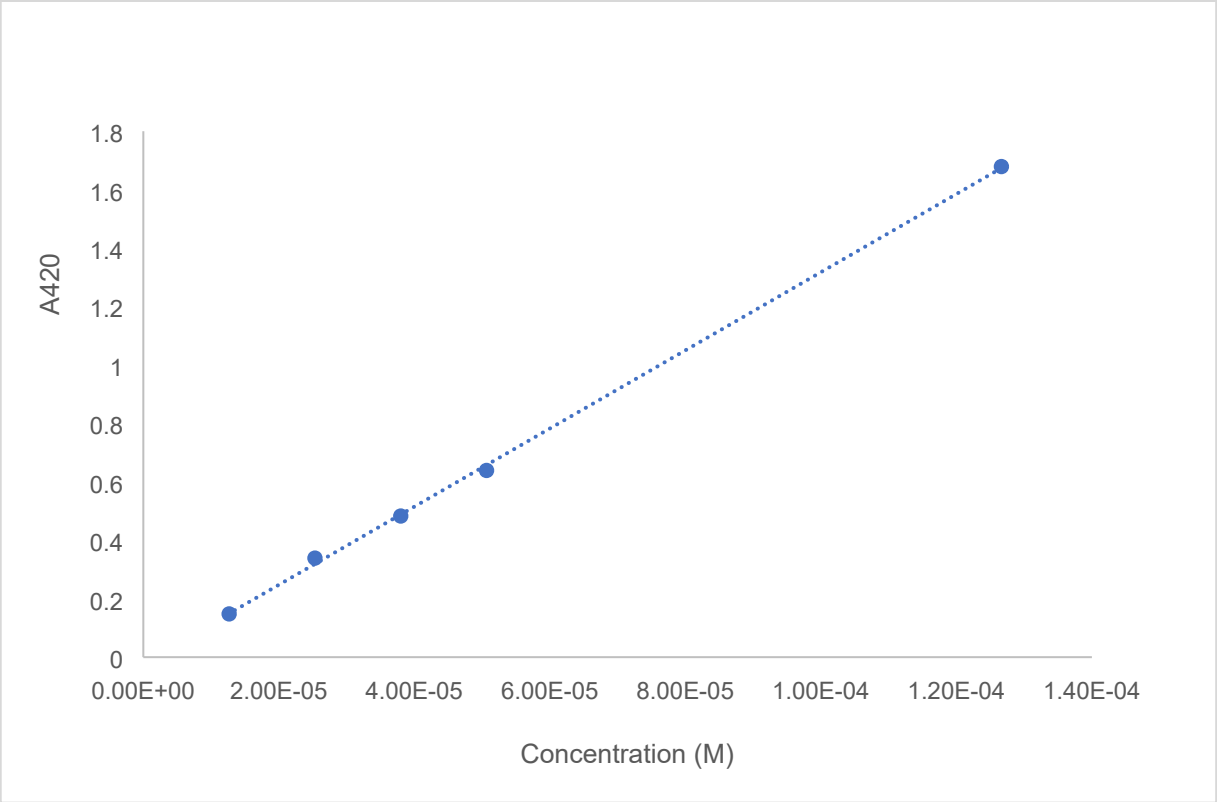

Figure S19. Beer's Law plot of **L1** in 1-octanol pre-equilibrated with pH 7.4 PBS at 420 nm.

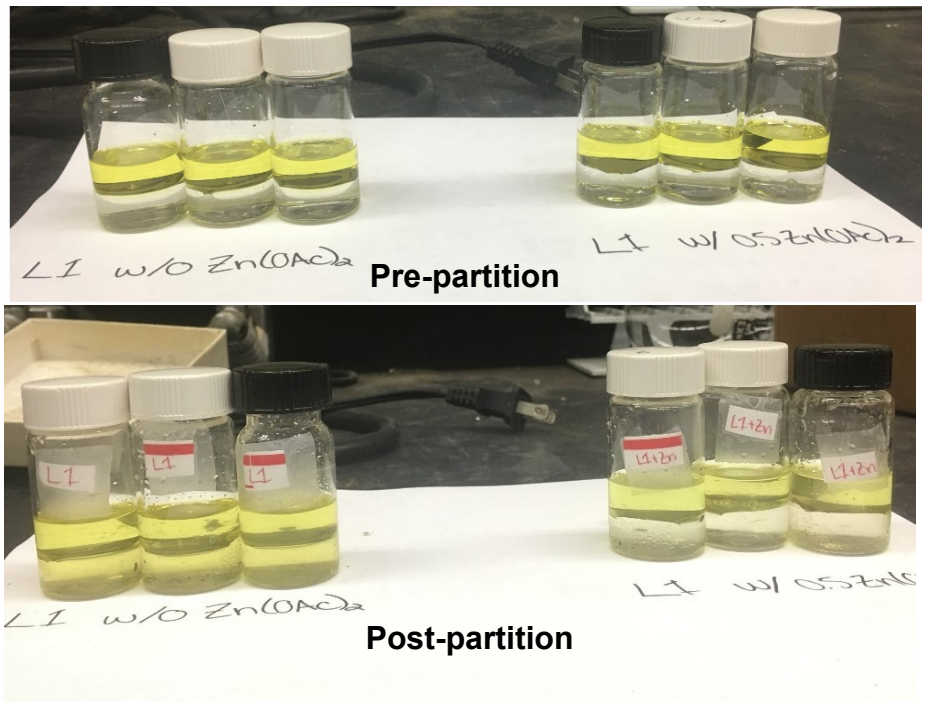

Figure S20. Picture of the vials containing **L1** dissolved in 1-octanol before (top) and after (bottom) shaking for 1 hour followed by separation of the phases. Vials on the left were shaken with an equal volume of PBS pH = 7.4 while those on the right were shaken with PBS containing 0.5 eq. of $Zn(OAc)_2$.

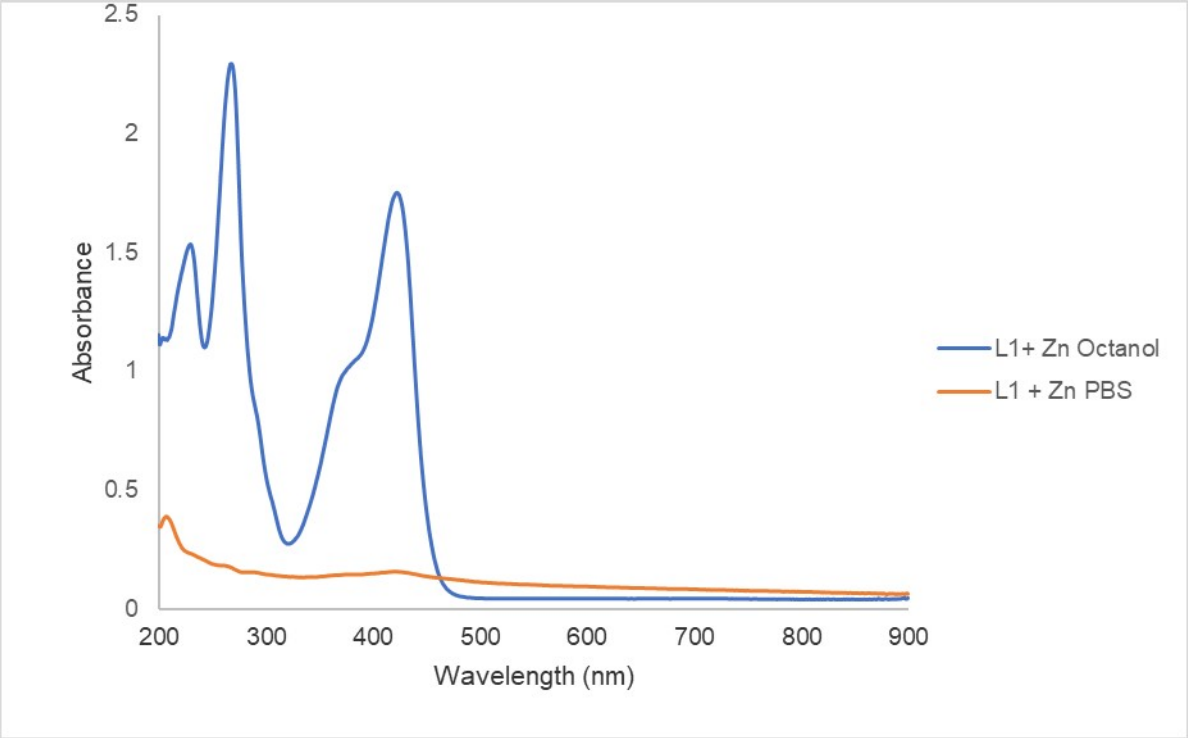

Figure S21. Overlay of UV-Vis spectra of 1-octanol layer before (blue) and after (orange) partition experiment with **L1** + 0.5 $Zn(OAc)_2$.

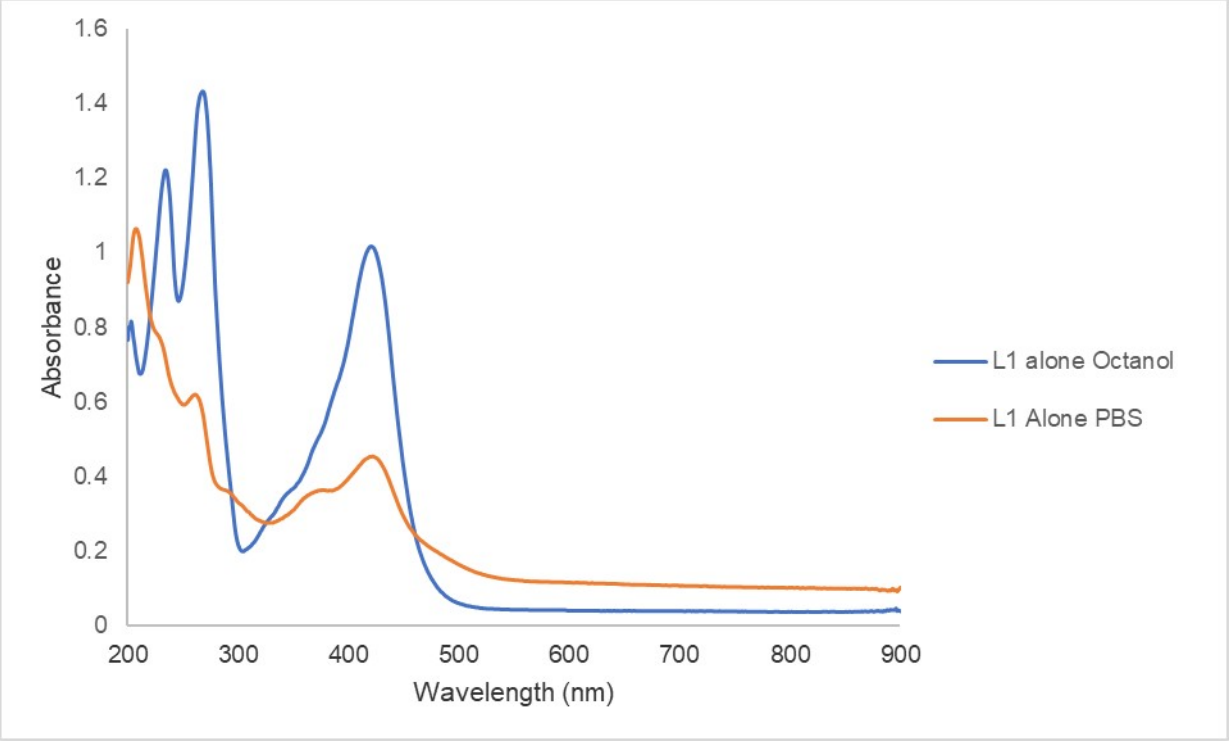

Figure S22. Overlay of UV-Vis spectra of 1-octanol layer before (blue) and after (orange) partition experiment with **L1** alone.

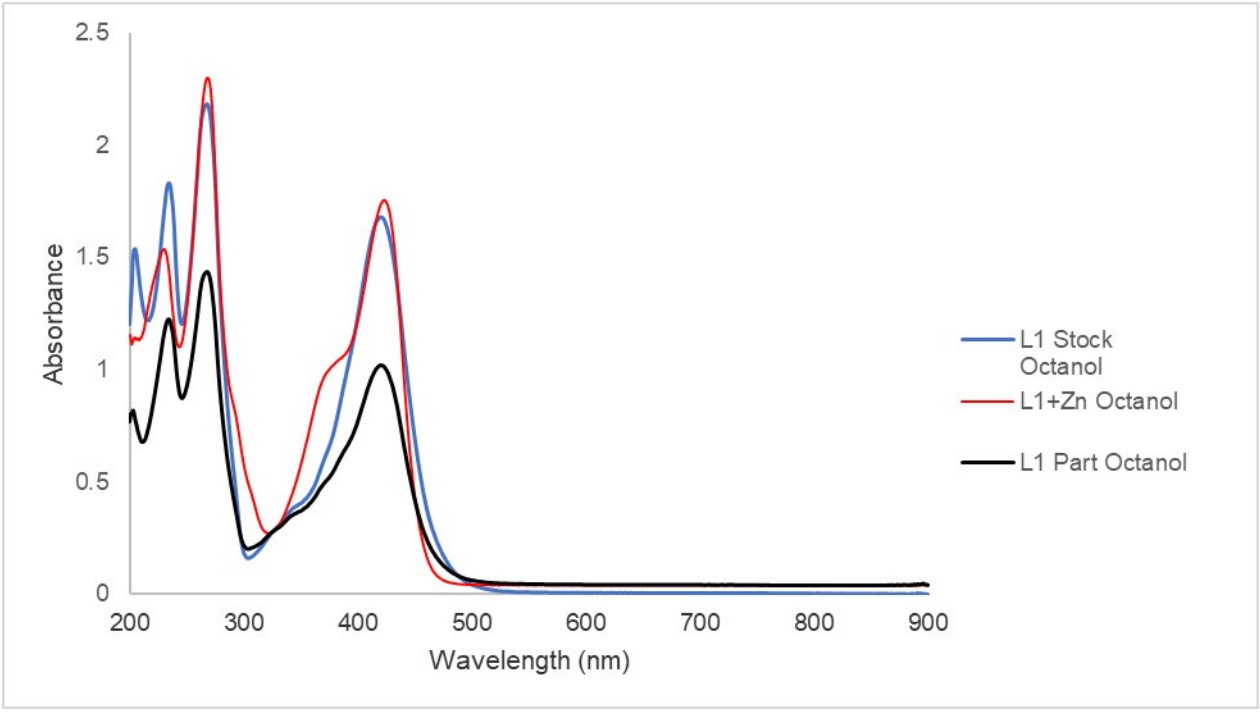

Figure S23. Overlay of UV-Vis spectra of 1-octanol layer before (blue) and after (red with Zn, black without Zn) partition experiment.

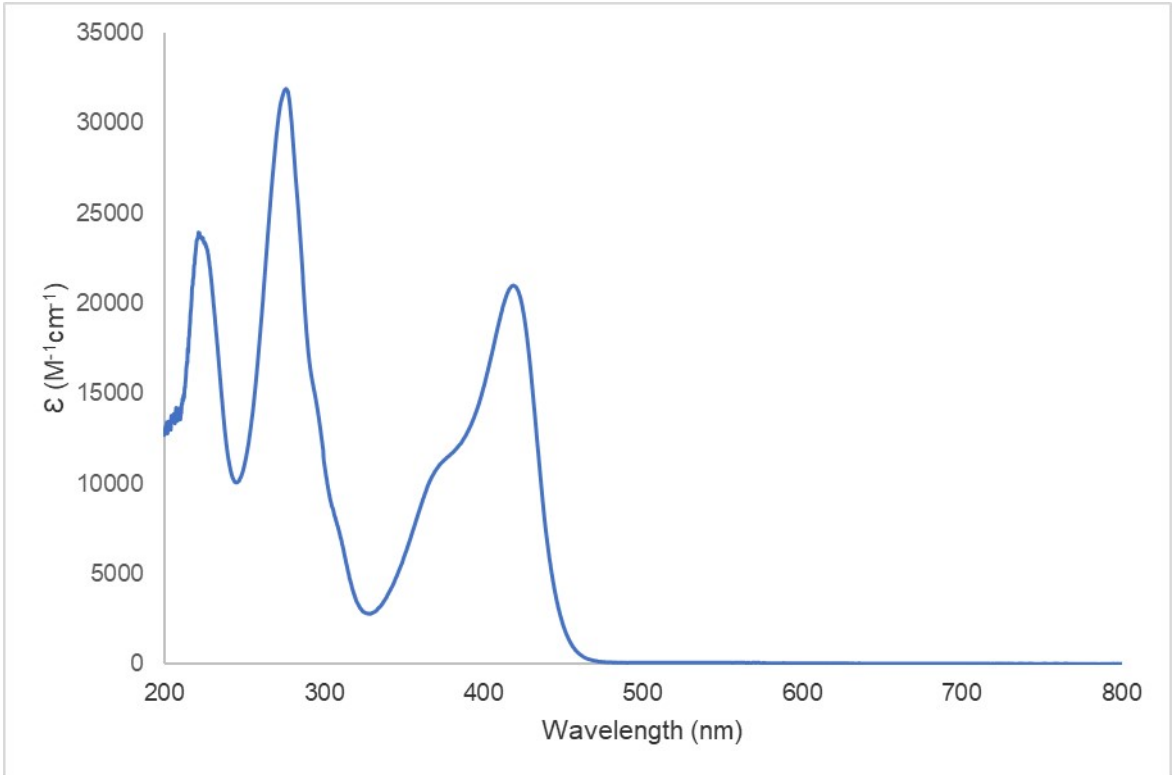

Figure S24. UV-Vis spectrum of Zn(**L1**)$_2$ solution in 1-octanol pre-equilibrated with pH 7.4 PBS.

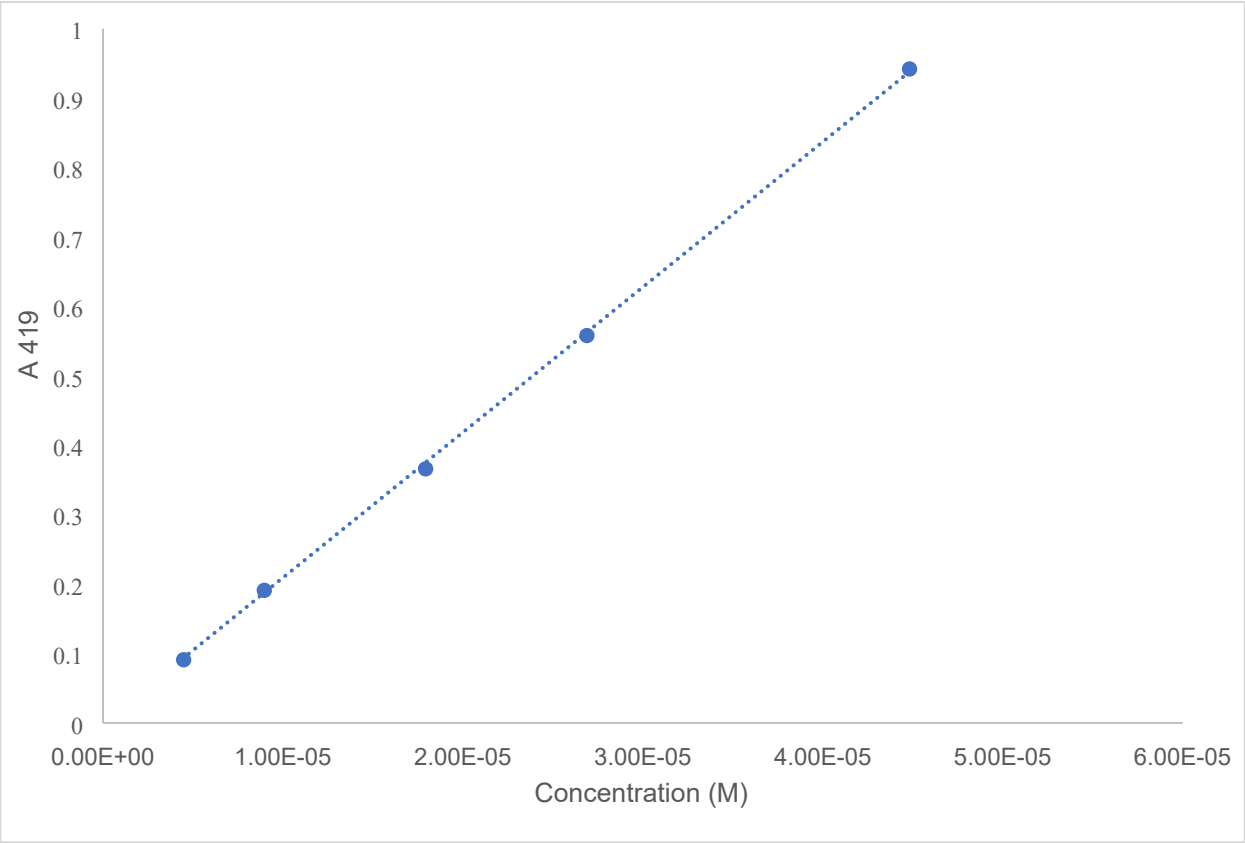

Figure S25. Beer's Law plot of Zn(**L1**)$_2$ in 1-octanol pre-equilibrated with pH 7.4 PBS.

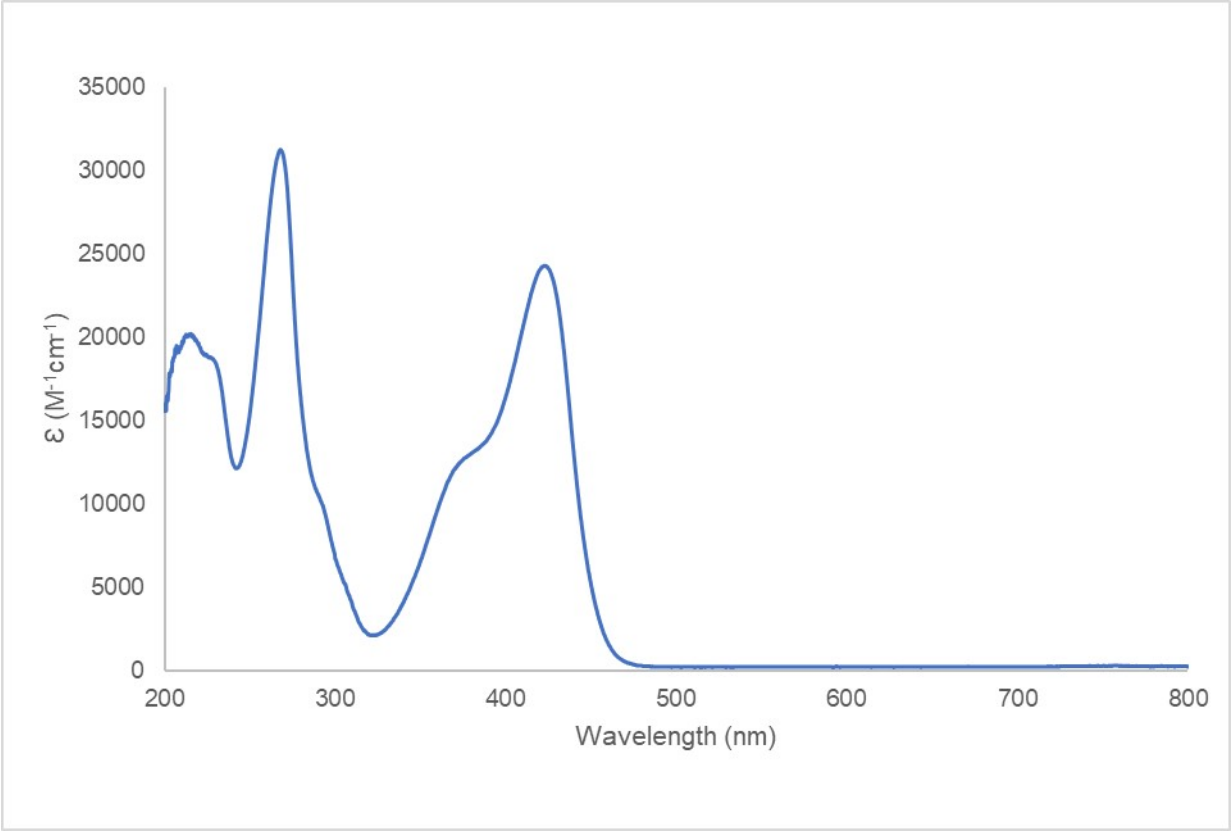

Figure S26. UV-Vis spectrum of Zn(**L2**)$_2$ solution in 1-octanol pre-equilibrated with pH 7.4 PBS.

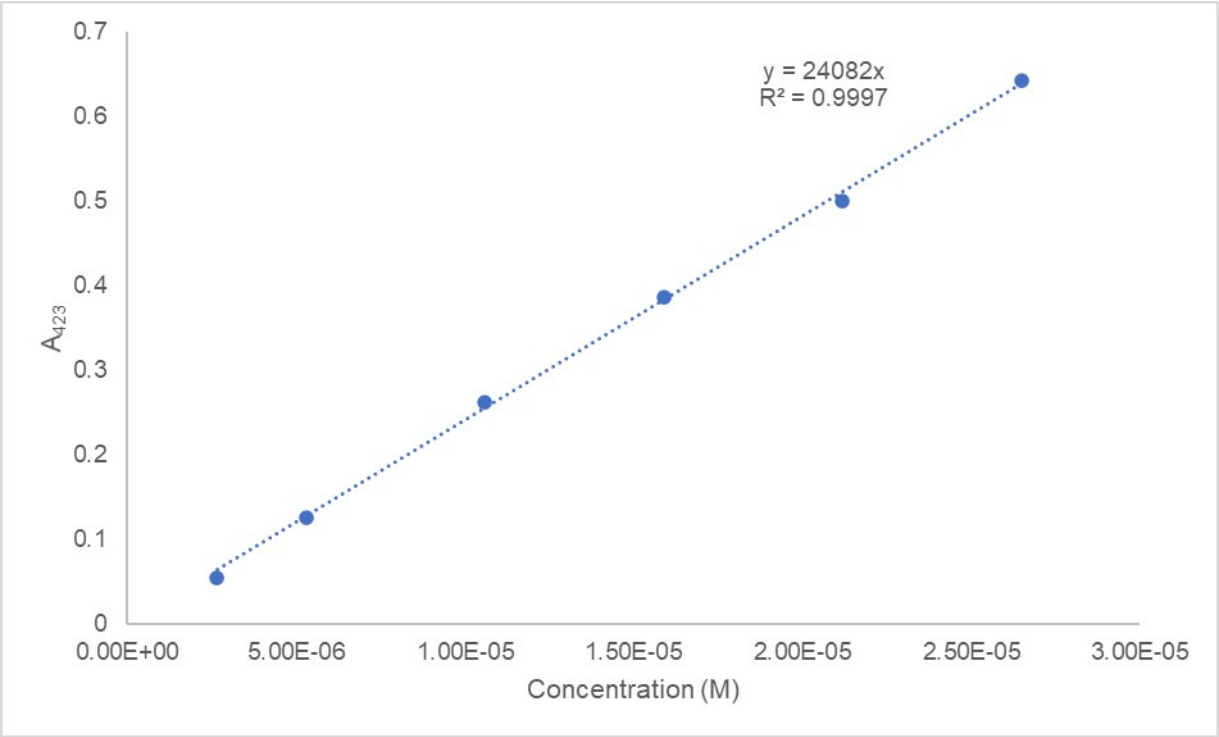

Figure S27. Beer's Law plot of Zn(**L2**)$_2$ in 1-octanol pre-equilibrated with pH 7.4 PBS at 423 nm.

Table S1. Summary of solution phase properties from UV-Vis. λ_{max} and Ɛ determined from DCM solutions.

Compound	λ_{max} (nm)	ε ($M^{-1}cm^{-1}$)	Λ_{max} (nm)	ε ($M^{-1}cm^{-1}$)	λ_{max} (nm)	ε ($M^{-1}cm^{-1}$)	$LogD_{7.4}$
L1	233	9360	269	11249	422	8813	0.36
Zn(L1)$_2$	230	21800	267	32326	416	27800	1.77
L2	232	16791	275	23487	421	15194	2.4[a]
Zn(L2)$_2$	232	20829	277	43004	413	30188	3.73

[a]Value from work by Elagawany et al.[4]

III. Crystal Structures of $Zn(L)_2$ complexes

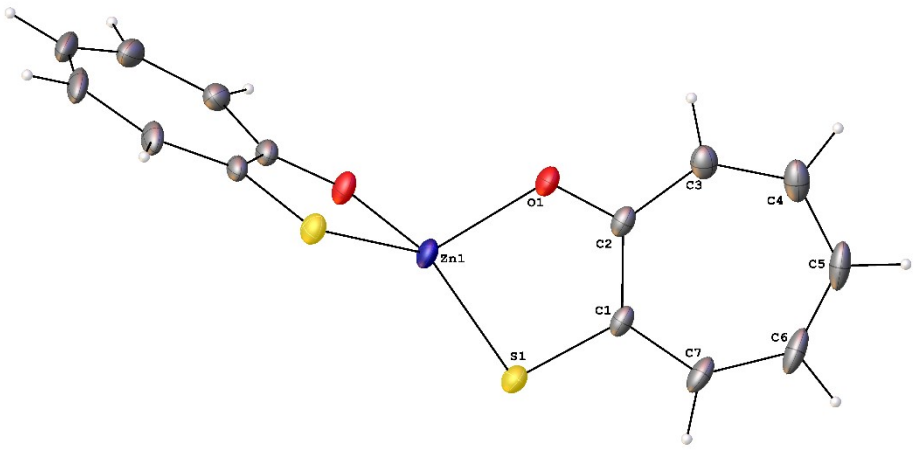

Figure S28. Crystal Structure of $Zn(\mathbf{L1})_2$

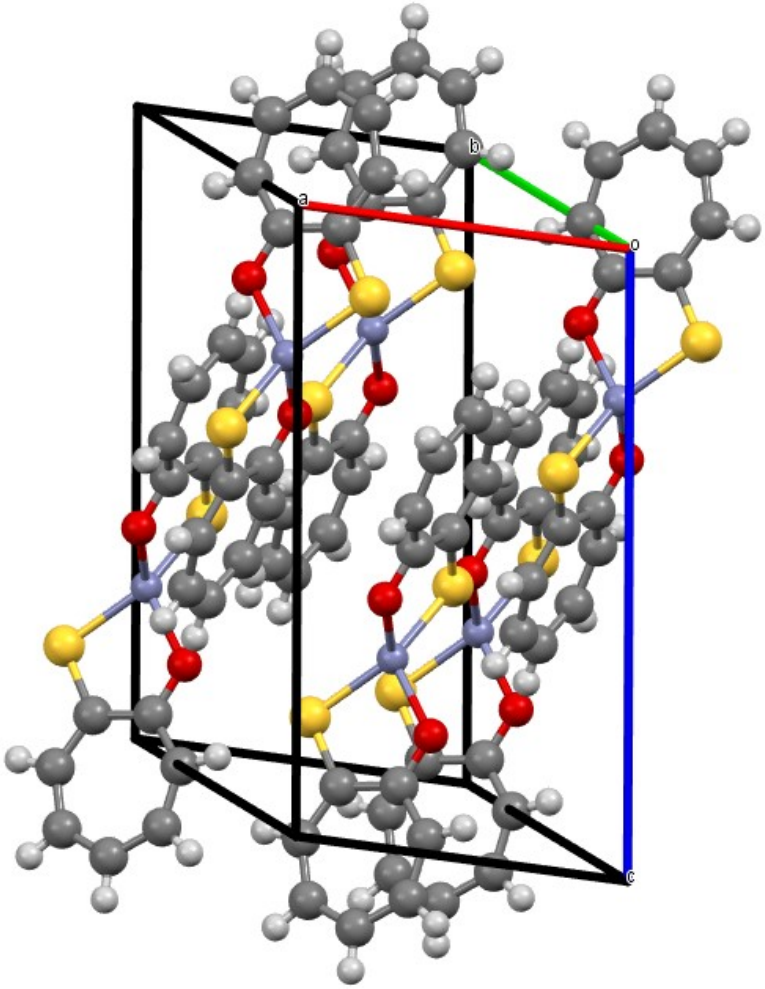

Figure S29. Packing diagram of Zn(**L1**)$_2$.

Table S2. Crystal data and structure refinement for Zn(**L1**)$_2$.

Identification code	zn2merc	
Empirical formula	C14 H10 O2 S2 Zn	
Formula weight	339.71	
Temperature	110.0 K	
Wavelength	0.71073 Å	
Crystal system	Monoclinic	
Space group	C 1 2/c 1	
Unit cell dimensions	a = 7.5612(6) Å	a= 90°.
	b = 12.5681(10) Å	b= 100.036(3)°.
	c = 13.8362(11) Å	g = 90°.
Volume	1294.73(18) Å^3	
Z	4	
Density (calculated)	1.743 Mg/m^3	
Absorption coefficient	2.211 mm^{-1}	
F(000)	688	
Crystal size	0.507 x 0.342 x 0.206 mm^3	
Theta range for data collection	2.990 to 33.106°.	
Index ranges	-11<=h<=11, -19<=k<=19, -21<=l<=21	
Reflections collected	22216	
Independent reflections	2400 [R(int) = 0.0491]	
Completeness to theta = 25.242°	99.4 %	
Absorption correction	Semi-empirical from equivalents	
Max. and min. transmission	0.3399 and 0.1826	
Refinement method	Full-matrix least-squares on F^2	
Data / restraints / parameters	2400 / 0 / 87	
Goodness-of-fit on F^2	1.192	
Final R indices [I>2sigma(I)]	R1 = 0.0499, wR2 = 0.1337	
R indices (all data)	R1 = 0.0534, wR2 = 0.1378	
Extinction coefficient	n/a	
Largest diff. peak and hole	1.444 and -0.559 e.Å^{-3}	

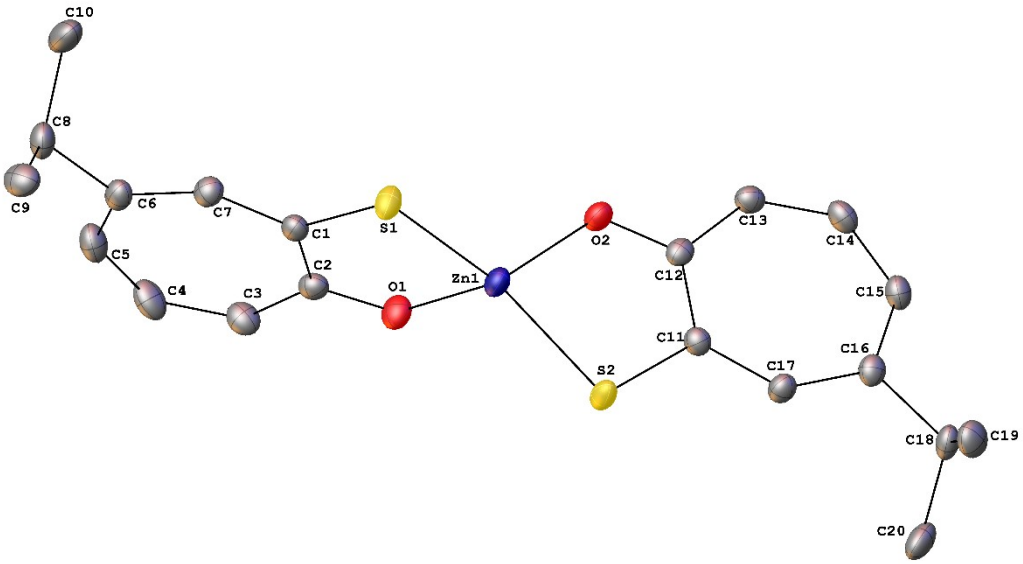

Figure S30. Crystal structure of Zn(**L2**)$_2$. Hydrogen atoms have been removed for clarity.

Figure S31. Packing diagram of Zn(**L2**)$_2$.

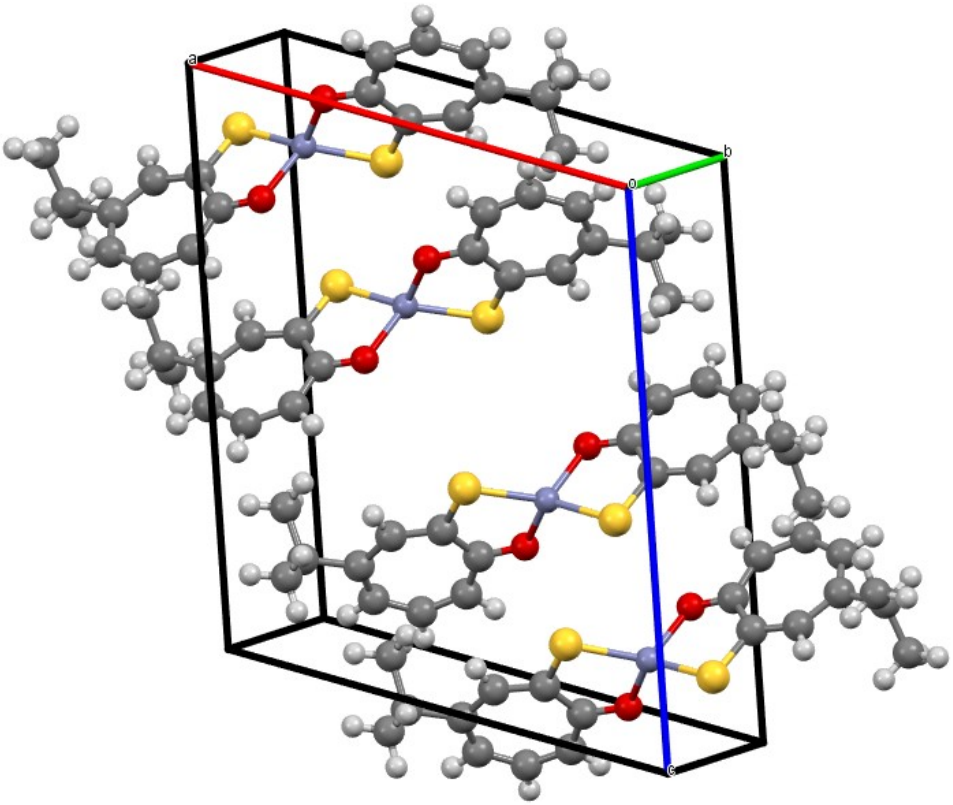
a
b
c
o

Table S3. Crystal data and structure refinement for Zn(**L2**)$_2$.

Identification code	znshk2	
Empirical formula	C20 H22 O2 S2 Zn	
Formula weight	423.86	
Temperature	110.0 K	
Wavelength	0.71073 Å	
Crystal system	Monoclinic	
Space group	P 1 21/n 1	
Unit cell dimensions	a = 12.4113(8) Å	a= 90°.
	b = 10.4092(7) Å	b= 108.298(2)°.
	c = 15.6036(10) Å	g = 90°.
Volume	1913.9(2) Å^3	
Z	4	
Density (calculated)	1.471 Mg/m^3	
Absorption coefficient	1.512 mm^{-1}	
F(000)	880	
Crystal size	0.402 x 0.043 x 0.039 mm^3	
Theta range for data collection	2.391 to 27.517°.	
Index ranges	-16<=h<=16, -13<=k<=13, -20<=l<=20	
Reflections collected	54898	
Independent reflections	4387 [R(int) = 0.0498]	
Completeness to theta = 25.242°	99.7 %	
Absorption correction	Semi-empirical from equivalents	
Max. and min. transmission	0.2616 and 0.1784	
Refinement method	Full-matrix least-squares on F^2	
Data / restraints / parameters	4387 / 0 / 230	
Goodness-of-fit on F^2	1.055	
Final R indices [I>2sigma(I)]	R1 = 0.0327, wR2 = 0.0762	
R indices (all data)	R1 = 0.0406, wR2 = 0.0808	
Extinction coefficient	n/a	
Largest diff. peak and hole	1.127 and -0.224 e.Å^{-3}	

Table S4. Hill slopes of inhibitory combinations used in this study from **Figure 4**.

Inhibitors	Hillslope	Inhibitors	Hillslope	Inhibitors	Hillslope
HK	-0.6 ± 0.6	0.5 μM HK + Zn	-3.4 ± 0.8	$Zn(HK)_2$	-1.4 ± 0.3
Trop	-1.7 ± 0.6	0.5 μM Trop + Zn	-2.5 ± 0.3	$Zn(Trop)_2$	-1.8 ± 0.3
L1	-3.7 ± 1.6	0.5 μM L1 + Zn	-1.3 ± 0.2	$Zn(L1)_2$	-2.0 ± 0.3
L2	-2.9 ± 0.6	0.5 μM L2 + Zn	-3.7 ± 0.8	$Zn(L2)_2$	-1.4 ± 0.3
				$Zn(NO_3)_2$	-1.8 ± 0.3

IV. Inhibition Studies

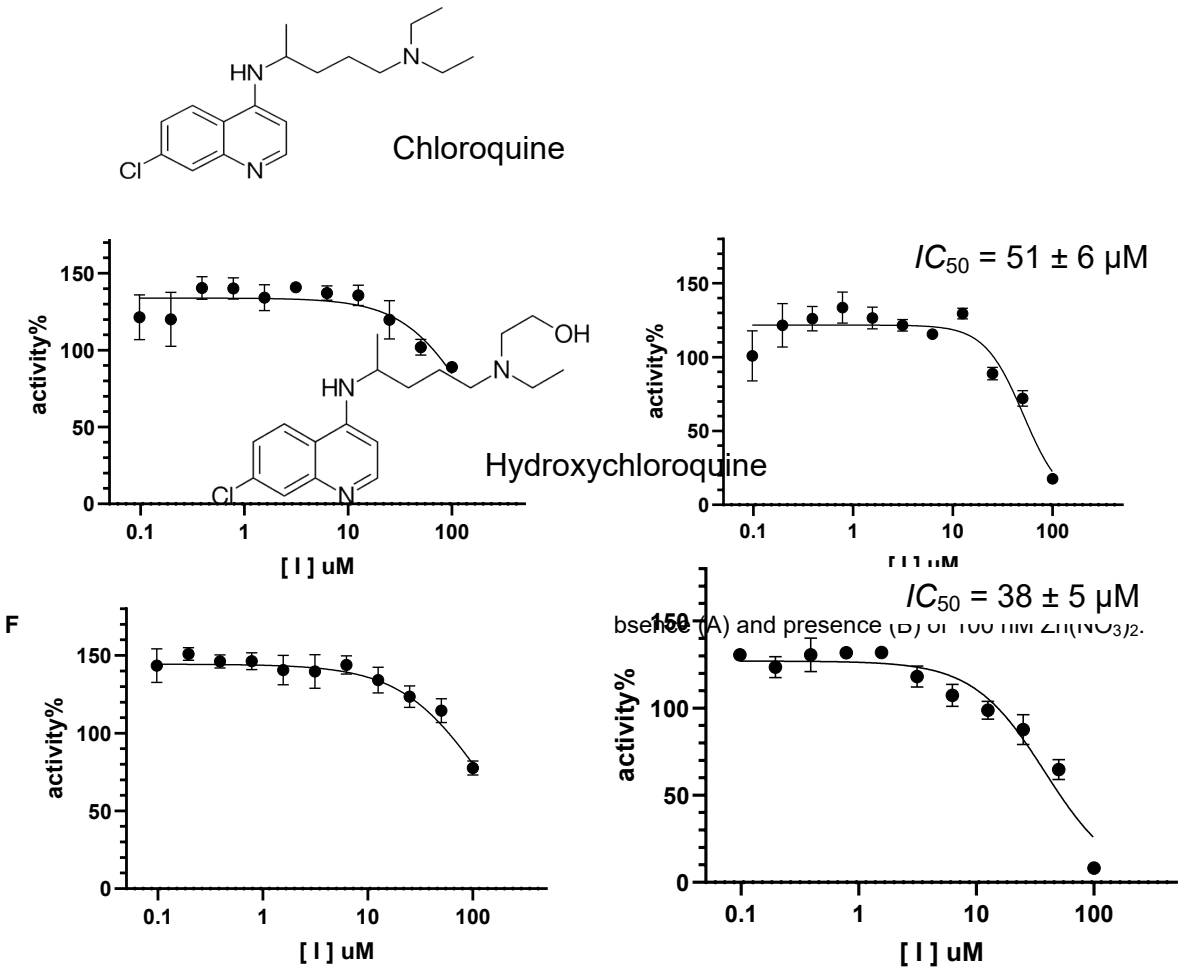

F bsence (A) and presence (B) of 100 nM $Zn(NO_3)_2$.

Figure S33. Inhibition of $SC2M^{pro}$ by hydroxychloroquine in the absence (A) and presence (B) of 100 nM $Zn(NO_3)_2$.

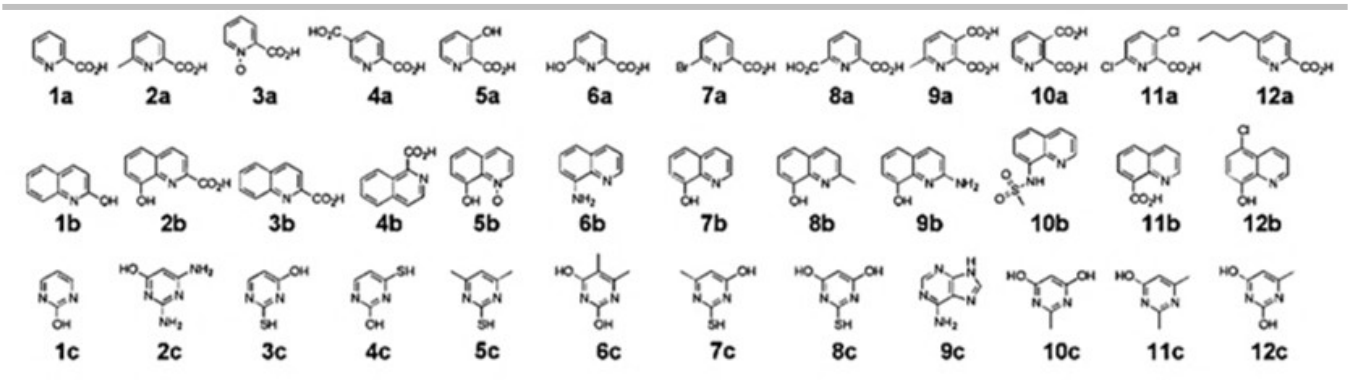

Figure S35. Library of Zn^{2+} ligands tested against SC2M^{pro}. Library adapted form Agrawal *et al*. [1]

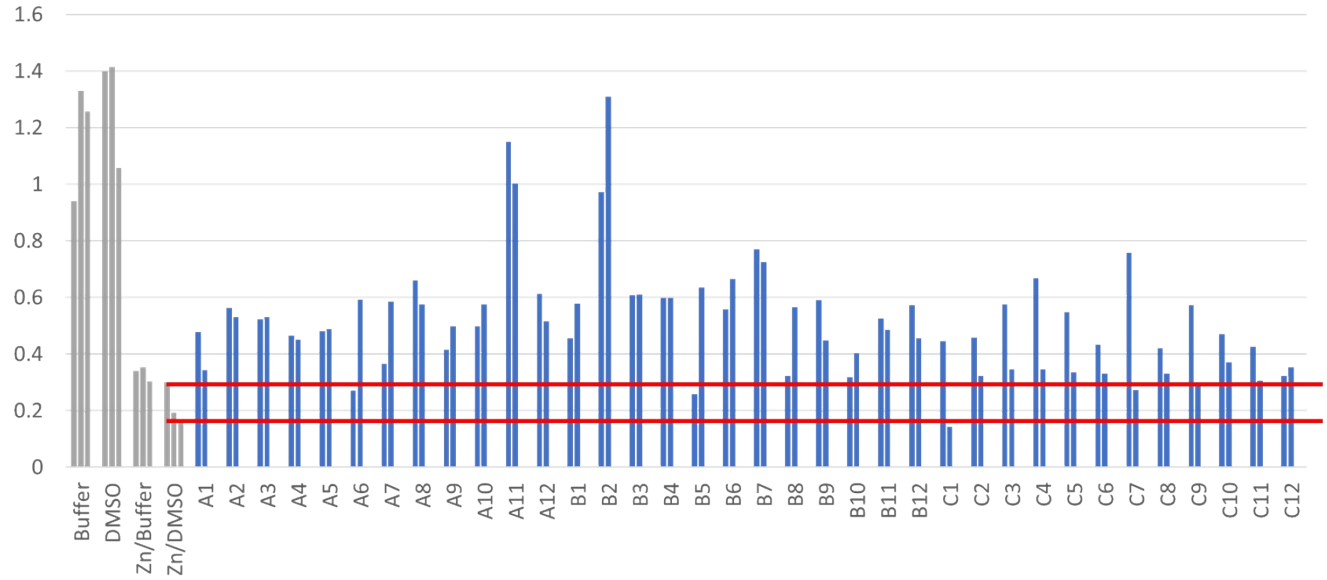

Figure S34. Initial screening of library of ligands at the outset of this study. Compound identity can be seen on the x-axis while relative activity can be seen on the y-axis. Each ligand was held at a concentration of 1 μM while [$Zn(NO_3)_2$] was 100 nM.. The red lines indicate the high and low bounds of 100 nM $Zn(NO_3)_2$. Values below the lines indicate an enhancement in inhibition of the Zn/ligand combination relative to $Zn(NO_3)_2$ alone.

V. Computational Studies

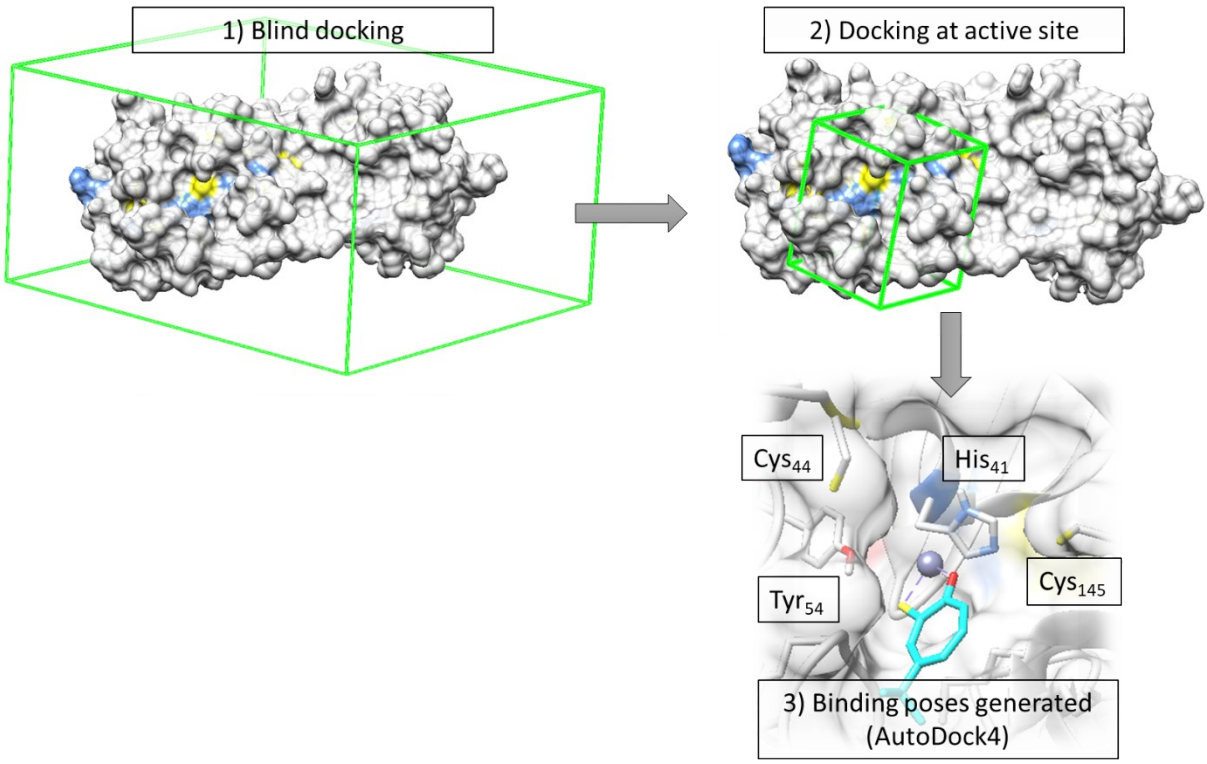

Scheme S1. Procedure used to generate proposed Zn(**L**)$_n$ binding poses on the M^{pro} monomer of SARS-CoV-2, with a AutoDock.[2] Residues in the active site that could potentially ligate to the Zn^{2+} complexes in this study are highlighted in panel 3.

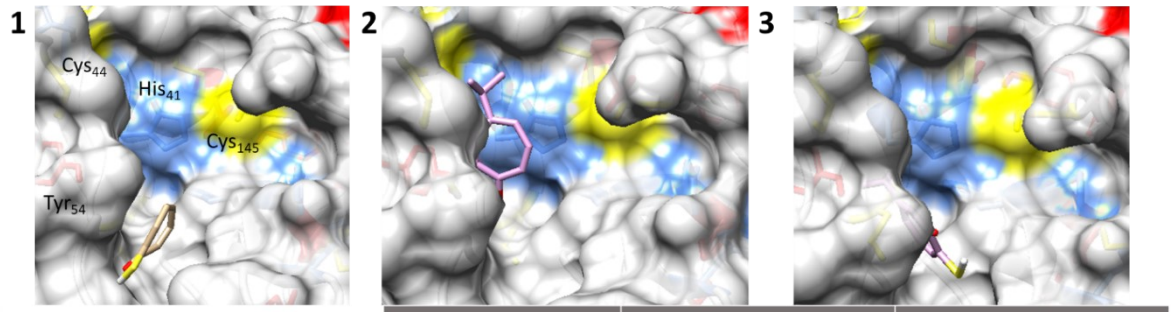

	1 (L1)	2 (L2)	3 (L3)
Estimated Free Energy of Binding	-4.06 kcal/mol	-4.77 kcal/mol	-4.23 kcal/mol
Final Intermolecular Energy	-4.36 kcal/mol	-5.37 kcal/mol	-4.83 kcal/mol
vdW + Hbond + desolv Energ	-4.29 kcal/mol	-5.34 kcal/mol	-4.79 kcal/mol
Electrostatic Energy	-0.07 kcal/mol	-0.03 kcal/mol	-0.04 kcal/mol
Final Total Internal Energy	-0.63 kcal/mol	-0.72 kcal/mol	-0.81 kcal/mol
Torsional Free Energy	+0.30 kcal/mol	+0.60 kcal/mol	+0.60 kcal/mol
Unbound System's Energy	-0.63 kcal/mol	-0.72 kcal/mol	-0.81 kcal/mol

Figure S36. Graphical representation of the binding pose with the lowest free energy generated using AutoDock4 for the free thiotropolone derivatives, 2-Mercaptotropolone (**L1**), 4-isopropyl-thiotropolone (**L2**), and 6-isopropyl-thiotropolone (**L3**). Relevant metal binding residues (Blue: histidine, Yellow: cysteine, Red: tyrosine) in the binding pocket are labeled using their three-letter abbreviation and sequence position in panel A, and are in analogous positions in panels B and C. Binding energies from the calculations are presented in the table below.

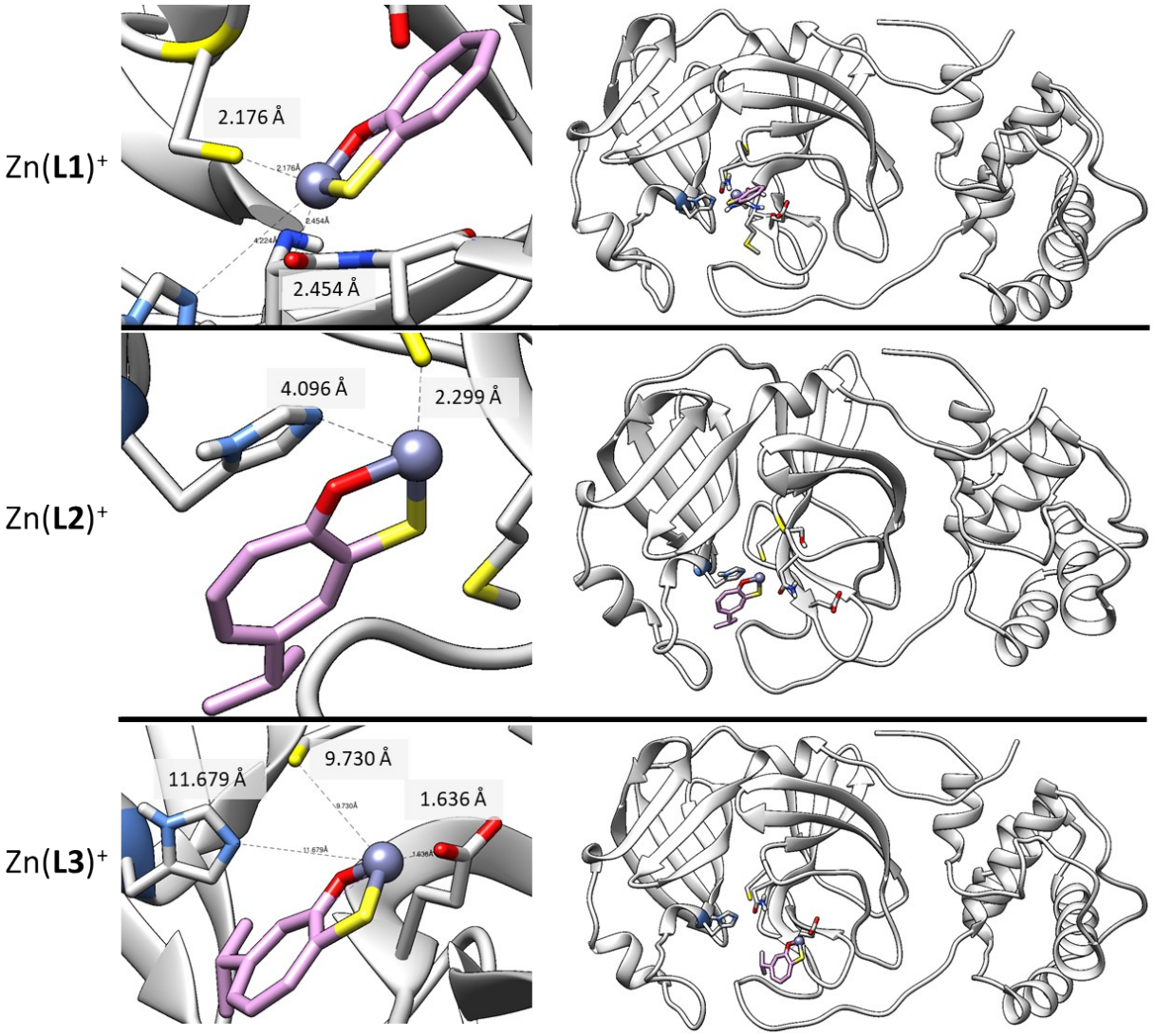

Figure S37. Graphical representations of Zn(**L1**)$^+$, Zn(**L2**)$^+$, and Zn(**L3**)$^+$ binding poses at the active site of the main protease of SARS-CoV-2 (PDB: 6W63). [Left] The zoomed-in binding region for the Zn fragments with bond distances shown in angstroms. [Right] Full view of the protein, indication association of the Zn(**L**)$^+$ fragment to the active site. Monomer portion of protein structure with inhibitor docked.

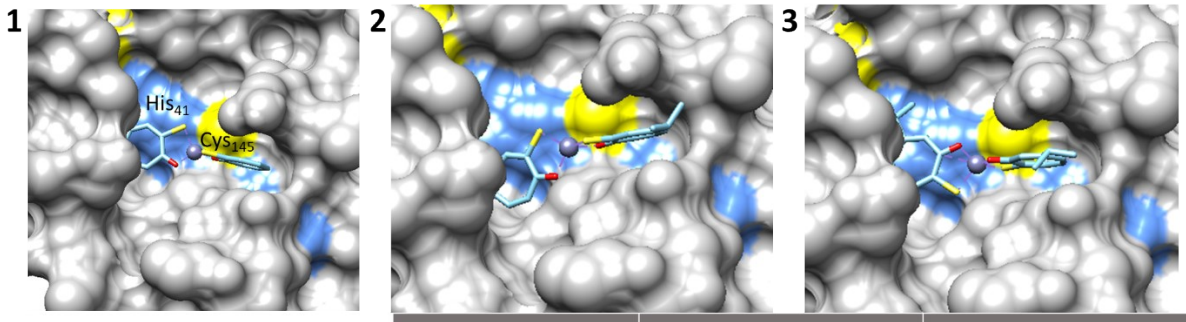

	(1) $Zn(L1)_2$	(2) $Zn(L2)_2$	(3) $Zn(L3)_2$
Estimated Free Energy of Binding	-6.75 kcal/mol	-7.66 kcal/mol	-7.07 kcal/mol
Final Intermolecular Energy	-6.75 kcal/mol	-8.26 kcal/mol	-7.67 kcal/mol
vdW + Hbond + desolv Energ	-6.74 kcal/mol	-8.23 kcal/mol	-7.64 kcal/mol
Electrostatic Energy	-0.01 kcal/mol	-0.03 kcal/mol	-0.03 kcal/mol
Final Total Internal Energy	-0.00 kcal/mol	-0.37 kcal/mol	-0.39 kcal/mol
Torsional Free Energy	+0.00 kcal/mol	+0.60 kcal/mol	+0.60 kcal/mol
Unbound System's Energy	-0.00 kcal/mol	-0.37 kcal/mol	-0.39 kcal/mol

Figure S39. Graphical representation of the binding poses with the lowest free energy generated using AutoDock4 for the bis-ligated Zn derivatives, Zn(**L1**)$_2$, Zn(**L2**)$_2$, and Zn(**L3**)$_2$. Relevant metal binding residues (Blue: histidine, Yellow: cysteine) in the binding pocket are labeled using their three-letter designator and sequence position in panel A, and are in analogous positions in panels B and C. Binding energies from the calculations are presented in the table below.

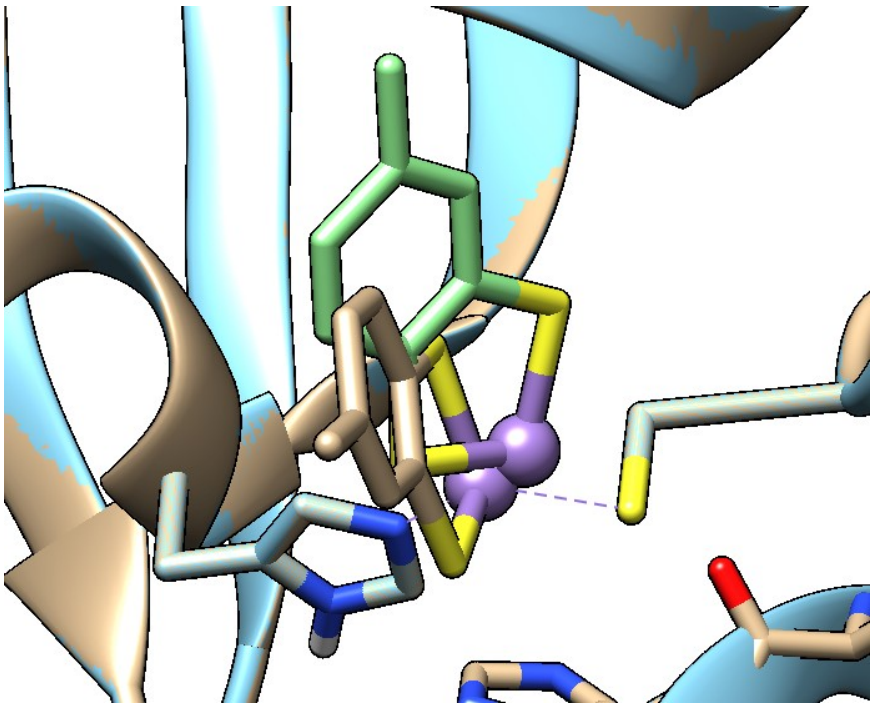

Figure S38. Binding poses generated from AutoDock4 calculations with Zn(TDT) [green] overlaid with the Zn fragment from the crystal structure [tan] (PDB: 2Z94). The catalytic dyad of His_{41} and Cys_{145} have been labelled for clarity.

VI. References

1. Agrawal, A.; Johnson, S. L.; Jacobsen, J. A.; Miller, M. T.; Chen, L.-H.; Pellecchia, M.; Cohen, S. M., Chelator Fragment Libraries for Targeting Metalloproteinases. *ChemMedChem* **2010,** *5* (2), 195-199.
2. Morris, G. M.; Huey, R.; Lindstrom, W.; Sanner, M. F.; Belew, R. K.; Goodsell, D. S.; Olson, A. J., AutoDock4 and AutoDockTools4: Automated Docking with Selective Receptor Flexibility. *J Comput Chem* **2009,** *30* (16), 2785-2791.
3. Murfin, L. C.; Weber, M.; Park, S. J.; Kim, W. T.; Lopez-Alled, C. M.; McMullin, C. L.; Pradaux-Caggiano, F.; Lyall, C. L.; Kociok-Kohn, G.; Wenk, J.; Bull, S. D.; Yoon, J.; Kim, H. M.; James, T. D.; Lewis, S. E., Azulene-Derived Fluorescent Probe for Bioimaging: Detection of Reactive Oxygen and Nitrogen Species by Two-Photon Microscopy. *J Am Chem Soc* **2019,** *141* (49), 19389-19396.
4. Elagawany, M.; Hegazy, L.; Cao, F.; Donlin, M. J.; Rath, N.; Tavis, J.; Elgendy, B., Identification of 4-isopropyl-thiotropolone as a novel anti-microbial: regioselective synthesis, NMR characterization, and biological evaluation. *Rsc Adv* **2018,** *8* (52), 29967-29975.
5. Murakami, H.; Yasui, H.; Yoshikawa, Y., Pharmacological and pharmacokinetic studies of anti-diabetic tropolonato-Zn(II) complexes with Zn(S(2)O(2)) coordination mode. *Chem Pharm Bull (Tokyo)* **2012,** *60* (9), 1096-104.
6. Barret, M. C.; Mahon, M. F.; Molloy, K. C.; Steed, J. W.; Wright, P., Synthesis and structural characterization of tin(II) and zinc(II) derivatives of cyclic alpha-hydroxyketones, including the structures of Sn(maltol)(2), Sn(tropolone)(2), Zn(tropolone)(2), and Zn(hinokitiol)(2). *Inorg Chem* **2001,** *40* (17), 4384-8.
7. Ting, R.; Lermer, L.; Perrin, D. M., Triggering DNAzymes with light: A photoactive C8 thioether-linked adenosine. *Journal of the American Chemical Society* **2004,** *126* (40), 12720-12721.
8. Andres, A.; Roses, M.; Rafols, C.; Bosch, E.; Espinosa, S.; Segarra, V.; Huerta, J. M., Setup and validation of shake-flask procedures for the determination of partition coefficients (logD) from low drug amounts. *Eur J Pharm Sci* **2015,** *76*, 181-91.
9. Vatansever, E. C.; Yang, K.; Kratch, K. C.; Drelich, A.; Cho, C. C.; Mellot, D. M.; Xu, S.; Tseng, C. K.; Liu, W. R., Targeting the SARS-CoV-2 Main Protease to Repurpose Drugs for COVID-19. *bioRxiv* **2020**.